Deformable plate tectonic models of the southern North Atlantic

Alexander L. Peace*[1], J. Kim Welford[1], Philip J. Ball[2] & Michael Nirrengarten[3]

[1] Department of Earth Sciences, Memorial University of Newfoundland, St. John's, Newfoundland and Labrador, A1B 3X5, Canada

[2] Faculty of Natural Sciences, Geography, Geology and the Environment, William Smith Building, Keele University, Newcastle, Staffordshire, ST5 5BG, United Kingdom

[3] Département Géosciences et Environnement, Université de Cergy-Pontoise, Neuville-sur-Oise, France

* Corresponding author. Email: alpeace@mun.ca

Abstract

Significant, poly-phase deformation occurred prior to, simultaneous with, and after the opening of the North Atlantic Ocean. Understanding this deformation history is essential for understanding the regional development and the mechanisms controlling rifting and subsequent failure or breakup. Here, we primarily use published constraints to construct deformable plate tectonic models for the southern North Atlantic from 200 Ma to present using GPlates. The aim of this work is to test both the capability of the GPlates deformable modelling approach and the reliability of published plate reconstructions. Overall, modelled crustal thickness values at 0 Ma produced from the deformable models show general, regional-scale, similarities with values derived from the inversion of gravity data for crustal thickness. However, the deformable models typically underestimate thinning in marginal basins and overestimate crustal thickness in continental fragments compared to values from gravity inversion. This is possibly due to: 1) thinning occurring earlier than the 200 Ma start time modelled, 2) variations in the original crustal thickness, 3) depth-dependent stretching, 4) rigid blocks undergoing some degree of thinning, and 5) variations in the mesh density of the models. The results demonstrate that inclusion of micro-continental fragments, and locally defined limits of continental crust, generally produce results more akin to observations. One exception is the Grand Banks where global GPlates models produce more realistic deformation, likely due to the inclusion of the exhumed domains continent-ward of the transition zone boundary. Results also indicate that Flemish Cap rotation is required to provide a reasonable fit between North America and Iberia, with the paleo-position of the Flemish Cap likely to be the proto-Orphan basins. Moreover, the East and West Orphan Basins formed separately due to the respective rotations of the Flemish Cap and the Orphan Knoll, which was likely associated with other continental fragments that subsequently contributed to the thicker crust forming the boundary between the East and West Orphan basins. The results also suggest a link between tectonic and magmatic processes. For example, the inclusion of an Orphan Knoll micro-continental block results in greater extension (higher beta factors) in the northern West Orphan Basin near the termination of the Charlie-Gibbs Fracture Zone, and the site of the Charlie-Gibbs Volcanic Province (CGVP). Thus, we infer that the CGVP was likely influenced by plate tectonic processes through the concentration of strain resulting from interaction in proximity

to the transform system. Finally, marginal basins that were considered to be conjugate and thus related, may only appear conjugate through later rotation of micro-continental blocks, and thus their genesis is not directly related.

Keywords

Rifting; Magmatism; North Atlantic; Deformable plate models; GPlates; Continental breakup; Tectonics; Plate Tectonic; Conjugate margins; Microplates; Rifted margins; Passive margins; Continental margins; Modelling; Crustal structure; Crust; Rift

Introduction

The opening of the modern North Atlantic Ocean represents the final dispersal and end of the Laurasia continental amalgamation that formed the northern portion of the Pangaea supercontinent (Gaina et al., 2009; Hansen et al., 2009; Frizon De Lamotte et al., 2015)(Fig. 1). The ocean is divided into two main spreading branches; the Northeast Atlantic between Greenland and Europe, and the Labrador Sea – Baffin Bay system between Greenland and North America (Srivastava, 1978; Beniest et al., 2017), that form a complex junction with the northeast Atlantic to the north of the Charlie-Gibbs Fracture Zone (CGFZ) (Gaina et al., 2009).

In addition to the primary breakup axes, complex styles of deformation occurred on the continental margins, including the preservation of relatively undeformed continental fragments (Peron-Pinvidic and Manatschal, 2010; Peron-Pinvidic et al., 2012; Nirrengarten et al., 2018; Schiffer et al., 2018), continental transform systems (e.g., the Davis Strait; Suckro et al., 2013; Peace et al., 2018a), and multiple failed rift axes (e.g., the North Sea; Rattey and Hayward, 1993). Despite the significant role that such deformation had upon the geological evolution of the continental margins, including the prospective petroliferous basins, plate tectonic reconstructions often struggle to account for much of this deformation prior to breakup (Ady and Whittaker, 2018). For this reason, it is the deformation in these continental rifted margins and basins, including the driving mechanisms, that form the focus of this study.

Here, we primarily use published constraints (e.g., Müller et al., 2016; Matthews et al., 2016; Nirrengarten et al., 2018; Welford et al., 2018) to construct deformable plate tectonic models for the southern North Atlantic using the open source GPlates environment (Williams et al., 2012a; Gurnis et al., 2018; Müller et al., 2018). We then compare the results obtained from the deformable models with both geological and geophysical observations including: crustal structure derived through gravity inversion (Welford et al., 2012; Roberts et al., 2018), regional seismic reflection lines (e.g., Tucholke et al., 2007; Tucholke and Sibuet, 2007), the age of syn-rift strata in passive margin rift basins (e.g., Gouiza et al., 2016), documented inversion (e.g., Yang, 2012), and occurrences of rift-related magmatism (e.g., Keen et al., 2014). The aim of this analysis was to investigate: 1) the reliability of published constraints as model components; 2) the reliability and applicability of the current generation of GPlates deformable models to reproduce realistic passive margin deformation, and 3) the implications for the spatio-temporal evolution of the region, including the consequences for magmatism, conjugate margin, and connected basin studies.

Background and Geological Setting

Geological Setting: the southern North Atlantic

In this study, the southern North Atlantic (Fig. 1) includes the conjugate Newfoundland-Iberia margins to the south and extends as far north as the southern Labrador Sea, southeast Greenland and the conjugate northwest European margin south of Iceland, approximately the same study area as that of Nirrengarten et al. (2018). This study area was chosen as the large-scale post-breakup plate movements are well constrained from studies of the oceanic crust (e.g., Barnett-Moore et al., 2018) and pre-breakup kinematics have been derived from studies of the surrounding rifted continental margins (e.g., Hopper et al., 2003; Gouiza et al., 2016; Dafoe et al., 2017; Nirrengarten et al., 2018; Peace et al., 2018b; Peace et al., 2018c; Gouiza and Paton, 2019), which provide constraints to build models of these domains.

Prior to breakup, the proto-North Atlantic region comprised a collage of Archaean and Proterozoic terranes (Kerr et al., 1996; St-Onge et al., 2009; Štolfová and Shannon, 2009; Engström and Klint, 2014; Grocott and McCaffrey, 2017). The breakup of the North Atlantic involved multiple rift and breakup phases (Srivastava, 1978; Lundin, 2002; Oakey and Chalmers, 2012; Barnett-Moore et al., 2018; Gernigon et al., 2019). Rifting prior to breakup of the North Atlantic is documented from the stratigraphic and magmatic record to have been multi-phase, and to have occurred from the Permian, been widespread during the Triassic, and continued into the Jurassic, Cretaceous and Cenozoic (Umpleby, 1979; Larsen et al., 2009; Stoker et al., 2016; Peace et al., 2018d). Following this prolonged, region-wide rifting, opening of the Atlantic was initiated in the Central Atlantic in the Jurassic and propagated into the proto-North Atlantic in Early Aptian time (e.g., Tucholke et al., 2007; Barnett-Moore et al., 2018).

Continental breakup resulted in the genesis of the North Atlantic ocean basin separating conjugate, rifted continental passive margins (Chian et al., 1995; Eddy et al., 2017; Gernigon et al., 2019). As with passive margins globally (Geoffroy et al., 2015; Franke, 2013; Lundin et al., 2018), North Atlantic passive margins can be considered to be 'magma-poor' such as the Grand Banks-Iberia, or 'magma-rich' such as the Rockall-Hatton Bank and southeast Greenland margins. However, significant widespread rift and breakup related magmatism is also documented on the so-called 'magma-poor' margins such as on and offshore Newfoundland (Strong and Harris, 1974; Lapointe, 1979; Deemer et al., 2010; Keen et al., 2014; Peace et al., 2017b; Peace et al., 2018c; Geng et al., 2019). Whilst the Newfoundland-Iberia margins are often considered as the archetypical 'magma-poor' margins (Peron-Pinvidic et al., 2007; Eddy et al., 2017; Alves and Cunha, 2018), the conjugate northern Newfoundland – Ireland conjugate pair has been the focus of fewer studies (Sinclair, 1995; Welford et al., 2012).

North Atlantic passive margins contain multiple rift basins that have attracted considerable petroleum exploration and production interest (Enachescu, 2006; Jauer et al., 2014; Alves et al., 2014; Scotchman et al., 2018; Schofield et al., 2018; Shannon, 2018), and thus it is of utmost importance that accurate plate reconstructions are produced with exploration in mind if they are to be useful in this aspect (Ady and Whittaker, 2018). In this study several of these marginal rift basins are focused on principally the Orphan Basin, offshore Newfoundland, Canada, and the Rockall and Porcupine basins, offshore the UK and Ireland, the development

of which are detailed in numerous previous works and as such only the most salient points are provided below.

The Orphan Basin

The Orphan Basin is located offshore NE Newfoundland (Figs. 1 & 2), on a predominantly non-volcanic segment of the Newfoundland passive margin (Reston, 2009). It is constrained by the continental shelf to the west, the Grand Banks to the south, the micro-continental fragments of the Orphan Knoll and Flemish Cap to the northeast and east, respectively and the Charlie-Gibbs fracture zone to the north (Peron-Pinvidic and Manatschal, 2010; Welford et al., 2012; Watremez et al., 2015; Gouiza et al., 2016; Dafoe et al., 2017) (Figs. 1 & 2). The Orphan Basin is considered to comprise of East and West sub-basins, separated by the Central Orphan High structure (Dafoe et al., 2017), a region comprising thicker crust (Welford et al., 2012). The basin was affected by several extensional episodes between the Jurassic and the Early Cretaceous, separated by events of uplift and erosion (Gouiza et al., 2016). The preserved tectono-stratigraphic sequences reveal that deformation initiated in the eastern part of the Orphan Basin in the Jurassic, followed by deformation in the west in the Early Cretaceous (Gouiza et al., 2015; Gouiza et al., 2016). This progression resulted in syn-rift structures filled with Jurassic–Lower Cretaceous syn-rift sediments that are overlain by thick Upper Cretaceous to Cenozoic post-rift sequences (Gouiza et al., 2016; Dafoe et al., 2017). Crucially however, it is likely the Cretaceous rifting that significantly thinned the crust and resulted in hyperextension in the basin (Gouiza et al., 2015; Lau et al., 2015).

The Porcupine Basin

The Porcupine Basin is a deep-water sedimentary basin, located offshore to the southwest of Ireland (e.g., O'Reilly et al., 2006; Watremez et al., 2018; Chen et al., 2018) (Fig. 1). Its present shape and large-scale structure formed through a major episode of lithospheric stretching in Jurassic times, with other rift episodes in earlier Permo-Triassic and later Early Cretaceous phases (Shannon, 1991; Tate, 1993; Sinclair et al., 1994; O'Reilly et al., 2006) resulting in hyperextension (Chen et al., 2018). The basin architecture is likely influenced by Caledonian trends (Doré et al., 1999). Constraints on the geometry of the pre-Cenozoic successions in the Porcupine Basin are poor away from the basin margins, with the Cretaceous and Mesozoic successions better understood as generally unfaulted and dominated by the post-rift interval (O'Reilly et al., 2006). A prominent, controversial, ridge feature has been documented in the southern part of the Porcupine Basin which has been interpreted as 1) a volcanic structure (Tate and Dobson, 1988; White et al., 1992; Calvès et al., 2012); 2) a serpentinite mud diapir (Reston et al., 2001, 2004); or 3) a block of continental crust (Hardy et al., 2010).

The Rockall Basin

The Rockall Basin is the sedimentary basin underlying the present day bathymetric depression known as the Rockall Trough offshore of the UK and Ireland (Fig. 1). The detailed geological evolution of the Rockall Basin is still largely unknown due to the lack of deep well penetrations in the basin and the limited seismic data coverage, leaving the early history of this vast region to be enigmatic (Tate et al., 1999; Shannon et al., 1999; Schofield et al., 2018; Roberts et al., 2018). Early extensional structures have been recognised, suggesting rifting initiated in the

Permo-Triassic, resulting in half-graben formation, followed by further extension in the Late Jurassic and Cretaceous (Doré et al., 1999; Naylor and Shannon, 2005). Igneous rocks are abundant in the Rockall Basin, particularly in the northeastern part of the basin where extensive flood basalt lava flows, sill complexes and volcanic centres of Late Cretaceous-to-Early Eocene age, belonging to the North Atlantic Igneous Province, have been described using seismic and borehole data (Archer et al., 2005; Thomson, 2005; Magee et al., 2014). In addition, the structure of the Rockall Basin is complicated further as the basin may have become hyperextended during Early Cretaceous rifting, leading to the potential for high segmentation, and a lack of Jurassic and older sequences towards the centre of the basin (Lundin and Doré, 2011). Regionally, there are similarities, including the correlation of key regional unconformities, between the Porcupine and Rockall basins, which demonstrate the similar history of these basins (McDonnell and Shannon, 2001).

Approach, materials, methodology and model setup

Reconstructions of the southern North Atlantic: the need for deformable plate tectonic models

Many plate tectonic models and reconstructions have been produced for the Mesozoic-Cenozoic rifting and breakup of the North Atlantic region (Bullard et al., 1965; Rowley and Lottes, 1988; Dunbar and Sawyer, 1989; Hosseinpour et al., 2013; Barnett-Moore et al., 2018; Nirrengarten et al., 2018). Each of these models inherently comes with its own assumptions, simplifications and omissions, depending on the scientific question being evaluated. Many, but not all (e.g., Whittaker, 2016; Ady and Whittaker, 2018), previous plate tectonic models for the southern North Atlantic are rigid-plate-type models and thus do not account for deformation of the continental domains prior to, during, and after breakup. The reason for this is that, although integral to deformation history, the constraints on deformation in the continental domains are much harder to obtain and less reliable compared to those from the oceanic domains such as dateable (and globally correlatable) oceanic magnetic anomalies and fracture zones (e.g., Srivastava and Roest, 1999). As such constraints do not exist for the deformed continental domains that this study seeks to reconstruct, alternative constraints must therefore be sought. Constraints on the deformation of continental domains can be obtained from 1) style and geometry of deformation including the locations of preserved continental fragments and large-scale faults, and 2) stratigraphic evidence for the timing of deformation, including rift-onset and termination (Nirrengarten et al., 2018). Finally, Although a global plate model that includes deformable plates was produced by Müller et al. (2019) here we focus on modelling different scenarios for the southern North Atlantic, and focus particularly on the role of microcontinental fragments.

Furthermore, deformation of adjacent continental domains must be resolved such that it is in agreement with the kinematics and timings of global models that have been derived from much better constraints of the oceanic crust (Seton et al., 2012; Matthews et al., 2016; Müller et al., 2016). In order to deal with this latter point, the GPlates deformable modelling approach that we utilised (Gurnis et al., 2018; Welford et al., 2018; Müller et al., 2019), primarily uses the large-scale movement of plates to drive deformation, in addition to the inclusion of micro-continental fragments in some models. Finally, as constraints on continental deformation are

much poorer, multiple scenarios must be considered, and thus modelled to evaluate their potential to accurately reproduce deformation.

The models presented in this work were built in GPlates 2.1 using the deformable plate modelling methodology and theory described in Gurnis et al. (2018) and deployed in Welford et al. (2018) to the Baffin Bay area, to the north of the primary study area in this work. The GPlates deformable plate modelling methodology allows for deformation to occur around surrounding rigid plates (Gurnis et al., 2018). Some deformable plate tectonic models are intended to accurately restore deformed crust (e.g., Ady and Whittaker, 2018). Here, however, the models are intended to examine the influence on deformation of variable input parameters. In particular, we investigate the roles of 1) preserved micro-continental fragments, 2) various interpretations of breakup timing and geometry, and 3) the timing of basin formation through nine different models intended to investigate sensitivity to specific input parameters. In this study, models that produce more similarity at 0 Ma with present day observations of crustal structure and deformation styles are deemed to be a better reconstruction of deformation, and thus their inputs are likely to be more accurate.

General model setup

We use the GPlates software (version 2.1) to conduct this investigation (e.g., Williams et al., 2012b; Müller et al., 2018). This open source plate tectonic modelling platform allows for a variety of investigations using plate tectonic reconstructions (e.g., Phethean et al., 2016; Gion et al., 2017) including deformable models (Gurnis et al., 2018; Welford et al., 2018).

Within GPlates 'features' (i.e. points, polylines or polygons) can be defined from geological and geophysical observations (Gurnis et al., 2018). Such features, optionally including their time of appearance and/or disappearance, can be combined into a topological network (Fig. 3). A topological network is a feature whose spatio-temporal evolution is defined by the features comprising the network (Müller et al., 2016). Within this evolving network in GPlates, crustal strain accumulation can be modelled (Fig. 4), and thus estimates of crustal thickness through time can be derived. The models can account for both thickening and thinning of the crust. The full methodology and governing equations behind the GPlates deformable models are provided in Gurnis et al. (2018) and applied in Welford et al. (2018) to Baffin Bay.

Here, through a series of models, we systematically change the components comprising a topological network of the southern North Atlantic in order to investigate their influence on crustal deformation. Specifically, nine different deformable plate tectonic models for the southern North Atlantic have been built, each of which is intended to test different input parameters (Table 1 and Fig. 5). All models were run from 200 Ma to the present (0 Ma) and assume a uniform, region-wide, crustal thickness of 30 km at 200 Ma, as this is within the range of values provided by previous studies (30-35 km thick) for the original crustal thickness of the Grand Banks, including the Flemish Cap (e.g. Marillier et al., 1994; Funck, 2003; Van Avendonk et al., 2009). Although widespread thinning likely occurred across the proto-North Atlantic region prior to 200 Ma, the modelled interval is taken as this time because prior to 200 Ma: 1) the reconstructions become increasingly unreliable due to the scarcity of oceanic crust, 2) the beta factors are generally too low, as there is no significant syn-rift fault heave (although

throw may still be significant e.g., Triassic faults in Jeanne d'Arc Basin; Tankard and Welsink, 1987) and, 3) the age of rift phases are poorly defined due to continental or lacustrine facies (Leleu et al., 2016). The implications of this assumption upon the results are discussed later in this paper.

Although our deformable models generally use inputs taken directly from the literature, minor modifications were required in some cases to: 1) test certain aspects of the inputs and their impact upon the results, and 2) to allow the models to run and produce geologically reasonable results. Where modifications from the previous versions were either required or experimented with, they are detailed below, as are the relevant models that have been produced with the original published version for comparison (Table 1). Crustal thickness points in GPlates were created for the entire deformable network in each model with a spacing of 1.15625° (GPlates density level 8) with no random offset.

The continent-ward extent of deformation

Studies of passive margins demonstrate that rift-related deformation may extend significant distances continent-ward of the first (oldest) oceanic or transitional crust (Wilson et al., 2006; Japsen et al., 2006; Ashby, 2013; Peace et al., 2018a; Peace et al., 2018c). Although such deformation generally likely decreases in magnitude continent-ward, the GPlates models require a solid boundary to denote the limits of deformation (Gurnis et al., 2018). As such, in all models presented in this work the outer limits of the topological network for the southern North Atlantic (i.e. the primary area of investigation) are taken to be the necking lines defined in Nirrengarten et al. (2018) based on the interpretation of crustal structure on seismic reflection-refraction lines and extrapolated with large-scale gravity inversion. In addition, although it is beyond the primary area of interest, the outer limits of deformation for the Baffin Bay – Labrador Sea area correspond to the 300 km half-width rift zone limits from Welford et al. (2018). Furthermore, the Nirrengarten et al. (2018) necking line has been extended further north along the southeast Greenland margin so that the Hatton-Rockall area could be examined. The addition of this continuation of the necking zone provides a boundary to the model but as it is not fully geologically constrained, detailed interpretation of the results on the East Greenland margin is not undertaken. The inclusion of the Baffin Bay – Labrador Sea area in addition to the southeast Greenland margin is primarily to provide a geologically reasonable northern boundary to the main study area to the south.

Finally, it should also be noted that Welford et al. (2018) found that the geometry and location of the outer limit of deformation is less important in controlling the resultant crustal thickness in the GPlates deformable models than other factors such as the timing of breakup. According to Welford et al. (2018) based on experiments with variable width of the rift zone, the main caveat is that the deformable zone needs to be wide enough so that edge effects do not have a significant influence. The continental margins defined by the topological networks were found to not be greatly influenced by edge effects and are of a similar width to those in Welford et al. (2018).

Extent of continental crust and timing of breakup

Model 1 uses the Müller et al. (2016) continent ocean boundaries (COBs) to define the ocean-ward limit of continental crust, whereas Models 2-6(a-d) use the edge of continental crust (ECC) from Nirrengarten et al. (2018). The Müller et al. (2016) COBs are taken from the global compilation and include exhumed mantle (hyper-extended) domains as material continent-ward of the COB (e.g., on the Grand Banks, offshore Newfoundland). The Nirrengarten et al. (2018) ECC on the other hand, is defined locally in the southern North Atlantic and places the exhumed domains ocean-ward of the. As the ECC and COB were defined independently by Nirrengarten et al. (2018) and Müller et al. (2016), respectively, it is important to recognise that the criteria used to define these domains is slightly different. The intent of using these different parameters in separate models was to investigate the influence of including the exhumed domains. The ECC was used as a model input rather than the last landward oceanic crust (LaLOC) (again from Nirrengarten et al. 2018) as LaLOC also includes the exhumed domains. In some areas however (e.g., on the northwest European margin), ECC and LaLOC from Nirrengarten et al. (2018) are at the same location. The reason for ambiguity in interpretation of some areas is partially due to high volumes of igneous intrusions hindering observations (Schofield et al., 2018), the interpreted absence of coupled and exhumed mantle domains, and the presence of compression, for example in northern Iberia (e.g., Druet et al., 2018).

The original ECC from Nirrengarten et al. (2018) does not include a defined time of appearance (i.e. breakup) in the same way that the Müller et al. (2016) COBs do, as the latter were compiled for use in reconstructions. Thus, times of appearance for the Nirrengarten et al. (2018) ECC were defined as corresponding to the times when the reconstructed ECC were no longer overlapping. Breakup times defined in this way can be seen in the results and do not differ greatly (within ~10 Myrs) from the ages of breakup for the adjacent Müller et al. (2016) COBs.

As such, the following times of appearance (breakup) for the Müller et al. (2016) COBs and the ECC modified from Nirrengarten et al. (2018) were used in the models (as detailed in Table 1):

- Newfoundland-Labrador margin – COBs appear at 126-110 Ma, and ECC appears at 140-120 Ma.
- Iberian margin – COBs appear at 130-124 Ma, and ECC appears at 140-120 Ma.
- Labrador Sea – COBs appear at 90-70 Ma, and ECC appears at 84-70 Ma.
- Bay of Biscay – COBs appear at 120 Ma, and ECC appears at 115 Ma.
- Southeast Greenland and conjugate Rockall-Hatton margin – COBs appear at 55 Ma, and ECC appears at 53.7-51 Ma
- Irish margin (Porcupine and southern Rockall) – COBs appear at 110 Ma and ECC appears at 115-83 Ma.

Finally, in order to achieve a more realistic time-progressive breakup, the Nirrengarten et al. (2018) ECC was broken up into much smaller polyline segments but the geometry was not greatly changed. The only area where the geometry had to undergo a minor amendment was for the Goban Spur and northwest Iberian margin to prevent overlap in the model that would not allow the mesh to be adequately constructed.

Poles of rotation

As with the majority of plate tectonic reconstructions, the GPlates environment poles of rotation are defined and used to reconstruct past plate movements and positions (Gurnis et al., 2012). Within the context of the models presented, it is the plate velocities derived through the poles of rotation relative to one another that drive deformation (Gurnis et al., 2018). Thus, it is essential that poles of rotation describe past plate motions as realistically as possible, and that multiple scenarios are considered. We therefore test multiple possible poles of rotation (reconstruction trees) including: 1) Matthews et al. (2016) (Model 1) 2) Nirrengarten et al. (2018) (Models 2-5), and 3) new poles of rotation (this study; for the Flemish Cap, Hatton-Rockall Bank, Porcupine bank and Orphan Knoll (Models 6a-d). The poles of rotation for the micro-continental blocks, including those derived in this study, are provided in Tables 2a-d and expanded upon in the subsequent sections. All features that lie on a particular plate (as defined by the GPlates static polygons; Müller et al., 2016) are rotated.

Micro-continental blocks and fragments

It is well-acknowledged that during rifting, fragments of continental material may remain relatively undeformed whilst the surrounding areas undergo significant deformation (Lister et al., 1986; Peron-Pinvidic and Manatschal, 2010; Blischke et al., 2011; Schiffer et al., 2018). A diverse range of preserved continental fragment types can be recognised and characterised including: micro-continents (e.g., Jan Mayen Microplate Complex; JMMC, Peron-Pinvidic et al., 2012a; Peron-Pinvidic et al., 2012b; Schiffer et al., 2018; Polteau et al., 2018), continental ribbons (e.g., Flemish Cap, Rockall Bank and Galicia Bank), H-Blocks (e.g., offshore Newfoundland), and extensional allochthons (e.g., ODP sites 1069, Iberian Margin) (Peron-Pinvidic and Manatschal, 2010).

As such, investigations into these relatively preserved fragments of continental material within the deformable rifted domain represent another significant element of the models. Nirrengarten et al. (2018) built a new regional plate tectonic reconstruction that included independent micro-continental blocks with individual temporally restricted poles of rotation. Specifically, the Nirrengarten et al. (2018) model includes polygons and temporally defined poles of rotation for the Flemish Cap, Orphan Knoll, Porcupine Bank and the Rockall-Hatton Bank. Thus, this new model allows for investigations into the development of the rift basins between these blocks of continental material during rifting to be undertaken. Furthermore, this model (i.e. Nirrengarten et al., 2018) therefore allows for a detailed investigation into the West and East Orphan, Rockall and Porcupine basins to be undertaken, where previous global reconstructions have not. In our models micro continental fragments behave as rigid blocks and retain their original (200 Ma) crustal thickness of 30 km throughout the modelled interval.

In addition to defining poles of rotation for the micro-continental blocks, the geometry of those features also had to be defined for the models. For the Flemish Cap and Porcupine Bank, the necking zone from Nirrengarten et al. (2018) was used, but as a separate feature from the main necking line (as outlined above). For the Hatton-Rockall Bank, the polygon from Nirrengarten et al. (2018) was used as a rigid block. The reason that the Rockall and Hatton Bank polygon was used rather than the necking zones was due to the many unknowns in the region, relating

to magmatic thickening of the crust obscuring the position of the necking domains and the likely influence of depth dependent stretching. For the Orphan Knoll, Model 1 uses the polygon from Nirrengarten et al. (2018) whilst Models 3 and 6a-d use a smaller polygon defined based-on the interpreted pre-rift basement on seismic reflection data (Fig. 2).

Individual model specifics and motivations

The input parameters for Models 1-6(a-d) are detailed in Tables 1 and 2a-d, and the initial setups for these models are shown on Figure 5, whilst descriptions of the intended line of investigation are provided below.

The intention of Model 1 was to investigate predictions for deformation when global constraints for poles of rotation and COBs (i.e. breakup ages) are used (Müller et al., 2016; Matthews et al., 2016). In global models of the Newfoundland and Iberian margins, the exhumed domains comprising serpentinised mantle peridotite are continent-ward of the COB. Model 1 does not include any micro-continental blocks so that their influence can also be isolated and thus assessed in the models where they are included. Model 2 was built to examine how the Nirrengarten et al. (2018) parameters would influence deformation without significant modification, whilst Model 3 is identical to Model 2 except that the geometry for the Orphan Knoll is defined using the basement horizon interpreted from seismic reflection data in the Orphan Basin (Fig. 2). Model 4 is the same as Models 2 and 3 except no micro-continental fragment for the Orphan Knoll is included. The only micro-continental fragment included in Model 5 is the Flemish Cap. The intention of Model 5 was to investigate deformation in the Orphan, Rockall and Porcupine basins in the absence of the smaller micro-continental fragments. Finally, the intention of Models 6a-d was to combine various components of the previous models (i.e. Models 1-5) that produced deformation most akin to geological and geophysical observations, in addition to experimenting with new poles of rotation that result in different configurations for the interplay between micro-continental fragments at 200 Ma.

GPlates deformable modelling results

Crustal thickness, evolution, and beta factors

The evolution of crustal thickness through time in all models shows general similarities as the large-scale movement of the major plates (i.e. North America, Greenland, Iberia and Eurasia) are ultimately driven by similar poles of rotation (e.g., Barnett-Moore et al., 2018). However, the small (basin) scale manifestations of deformation are highly variable. Implications for this deformation form the focus of this study and are more susceptible to minor variations in model inputs such as micro-continental fragment parameters.

In this section, where appropriate, the results for particular regions have been grouped into scenarios that contain similar results, as not all aspects are varied in each model, allowing for the isolation of controlling mechanisms (Table 1). The results of the crustal thickness modelling are shown in Figures 6 and 10 for the entire modelled region, and for the Irish and Canadian margins in Figures 11 and 12, respectively. The results of the extension (beta factor) calculations for the deformable models are shown for the Irish and Canadian margins in Figures 13 and 14, respectively. Beta factors for the entire modelled region are provided in the

supplementary information. For all beta factor calculations, an initial model (200 Ma) crustal thickness of 30 km was assumed (Table 1).

Porcupine Bank and Basin

The region in proximity to the Porcupine Bank and Basin represents one of the areas that the different models produced highly variable results, in terms of both the final crustal thickness (0 Ma; Figs. 6 and 11) and evolution from 200 Ma (Figs. 5-7), in addition to the calculated beta factors (Figs. 13 and 14). This demonstrates the importance of microcontinental fragments in the rift evolution of this region. Moreover, although nine models are presented in this study (Fig. 4), these only result in three significantly different scenarios for the Porcupine Basin as a result of differing amounts (or absence) of rotation of the Porcupine Bank (Table 1). For the crustal thickness in the Porcupine Basin, these are: scenario 1 (no thinning; Models 1 and 5), scenario 2 (moderate crustal thinning to approximately 20 km at 0 Ma; Models 2, 3 and 4), and scenario 3 (significant crustal thinning to approximately 5-15 km at 0 Ma; Models 6a, 6b, 6c and 6d) (Figs. 6 and 11).

In scenario 1, with no relative movement between the Porcupine Bank and the Irish margin necking zones, no deformation occurs in the Porcupine Basin for the entire modelled interval between 200 and 0 Ma (Figs. 6a,e, 5a,e, 6a,e and 7a,e). In such a situation, the Porcupine Basin is essentially protected from deformation elsewhere due to its unique shaped geometry, resulting in beta factors of 0 (Figs. 13a,e). In scenario 2, by 150 Ma, thinning of the crust in the Porcupine Basin is apparent, resulting in crust in the southernmost Porcupine Basin that is down to 20 km thick but minimal crustal thinning in the northern parts of the Porcupine Basin (Fig. 9b, c & d). Crustal thicknesses established at 150 Ma in scenario 2 remain unchanged until present (0 Ma) due to the cessation of clockwise rotation of the Porcupine Bank, giving beta factors of 2-4 (Figs. 13b-e). In scenario 3, more significant rotation of the Porcupine Bank (compared to the models in scenario 2) results in much thinner crust at 150 Ma in the Porcupine Basin of approximately 5-20 km (Fig. 9f-i). By 100 Ma in scenario 3, thinning is widespread in the Porcupine Basin with crustal thickness generally < 15 km (Fig. 8f-i) and beta factors of approximately 4-6 (Fig. 13f-I, i.e. hyperextension), with regional thin-spots in the north and south depicting crustal thicknesses as low as 5 km (Fig. 11f-i) and beta factors of 6-8 (Fig. 13f-i). In scenario 3, the crustal thicknesses (and therefore beta factors) predicted at 100 Ma continue until present (0 Ma) (Fig. 6f-i & 11f-i).

The Orphan Basin

As with the Porcupine Bank and Basin area (Fig. 1), the Orphan Basin (Fig. 2) represents one of the areas in this study that the different models produce highly dissimilar results, again in terms of both the final crustal thickness (0 Ma; Fig. 6 & 12), and temporal evolution from 200 Ma (Fig. 7-8), in addition to beta factor calculations (Fig. 14). This is as a result of the focus on the role of the Orphan Knoll and Flemish Cap micro-continental fragments during rifting, and in particular their paleo-positions, geometries and trajectories to their current locations, which profoundly influenced the crustal development of the Orphan Basin.

In Model 1, at 200 Ma, it can be seen that the necking zone for the Flemish Cap overlaps with the necking zone on the Iberian margin (Fig. 4a), an unrealistic phenomena that is discussed in

detail below. Furthermore, by 0 Ma in Model 1, with no relative movement between the North American necking zone and the Flemish Cap, crustal thicknesses are maintained at approximately 30, 25, and 20 km in the southernmost, central, and northernmost Orphan Basin, respectively (Figs. 6a & 12a), resulting in beta factors near 0 for much of the Orphan Basin (Fig. 14a). This is particularly apparent at 100 Ma (Figs. 8a) where it can be seen that relative movement between North America and Europe results in some thinning in the outermost Orphan Basin but minimal effects towards the North American necking zone where the inner Orphan Basin is essentially protected from thinning.

In Model 2, the use of the more extensive Nirrengarten et al. (2018) geometry for the Orphan Knoll results in crustal thickness variations in the Orphan Basin at 0 Ma from 5-25 km (Figs. 6b & 12b) and beta factors of approximately 2-6 (Fig. 14b). Furthermore, a significant dichotomy between the extent of deformation in the East and West Orphan sub-basins is apparent in Model 2. In particular, at 0 Ma, significantly thinner crust of <10-15 km is predicted in the West Orphan Basin (beta factors of 4-6) compared to the East Orphan Basin where 15-20 km thick crust (beta factors of 2-4) is predicted. In addition, particularly thin crust of < 5 km thick (beta factors 6-8) is modelled at 0 Ma in the northernmost West Orphan Basin. Model 2 predicts thinning of the East Orphan Basin earlier than the West Orphan Basin, which can be observed at 150 Ma (Fig. 9b) where crust of approximately 30 km is still underlying the West Orphan Basin whilst the East Orphan Basin has been thinned to approximately 20 km thick crust. Overall, Model 2 predicts significantly thinner final (0 Ma) crustal thickness and earlier thinning in the East than the West Orphan sub-basins.

Model 3 used a smaller spatial extent for the Orphan Knoll (Figs. 2 and 4c) but the same poles of rotation as those used in Model 2 (Table 1). The result of this is that at 0 Ma, a region of crust approximately 15-20 km thick (beta factor <2; Fig. 14c) persists from the western Flemish Cap to the western limits of the Orphan Basin that is not apparent from the Model 2 results (Figs. 12c). Furthermore, the differing crustal thicknesses between the East and West Orphan sub-basins (as predicted by Model 2) are not apparent. However, the earlier thinning of East Orphan (Fig. 9c) is still apparent.

The evolution of crustal thickness in Models 4 and 5 is very similar as the inputs for the Orphan region are the same (Table 1). In Models 4 and 5, the absence of an Orphan Knoll plate (Fig. 4) and the inclusion of the Flemish Cap rotation results in more uniform crustal thicknesses across the Orphan Basin (Fig. 12d-e), with less of the small-scale manifestations of deformation observed in this region in other models (e.g., Models 2, 3 and 6a-d). In particular, at 0 Ma, crust of 10-15 km thick (beta factor approximately 4; Fig. 14d) is predicted in the northwest, with a band of crust approximately 15-20 km thick (beta factor predominantly < 3; Fig. 14d) across the central Orphan Basin and a particularly thin region of crust around 5 km thick (beta factor approximately 6; Fig. 14d) in the southernmost Orphan Basin.

Models 6a-d all include the Orphan Knoll and Flemish Cap as independent plates but with variable starting (200 Ma) positions and subsequent trajectories (Table 1 & Fig. 4f-i). The result of modifying the starting positions and trajectories of the Orphan Knoll and Flemish Cap is that Models 6a-6d display highly variable crustal evolution and final results, demonstrating the importance of these micro-continental fragments, as discussed below.

In Model 6a, the Flemish Cap is located close to the North American margin necking zone whilst the Orphan Knoll is located outboard, northwest of the Flemish cap (Fig. 4f). This configuration results in extensive rapid crustal thinning from 200-150 Ma between the Orphan Knoll and Flemish Cap down to < 5 km thickness, and crustal thinning down to 15 km for the rest of the East Orphan Basin (Fig. 9f). By 100 Ma, Model 6a predicts crust approximately 5-10 km thick (beta factor of approximately 4-6) for the majority of both the East and West Orphan sub-basins, with the easternmost parts of the West and East Orphan basins displaying crust < 5 km thick (beta factor > 15), which remains the case until present (Figs. 6f, 12f & 14f).

In Model 6b, the Orphan Knoll is initially located south of its position in Model 6a, west of the Flemish Cap (Fig. 4g & Table 1). The result of this configuration is that, of all the model results, it is Model 6b that produced the most extensive thinning across both the East and West Orphan basins (Figs. 12 and 14). In particular, this extensive thinning was established by 150 Ma when crust approximately 5-10 km thick (beta factor 3-6) is predicted in the East Orphan Basin (Fig. 9g). By 100 Ma, Model 6b predicts crust 5-10 km thick (beta factor 3-6) across the entirety of both the East and West Orphan basins (Fig. 8g), which persists until present (Fig. 6g & 12g).

The Orphan Knoll in Model 6c is again initially located west of the Flemish Cap, however, both the Flemish Cap and the Orphan Knoll are not as tightly positioned next to the North American margin necking zone (Fig. 4h). The result of this initial plate tectonic configuration is that by 150 Ma, most of the crust in the East Orphan Basin has been thinned to 15 km (beta factor 2), with localised areas depicting <10 km thick crust (beta factor 3) such as south of the Orphan Knoll (Fig. 9h). By 100 Ma in Model 6c, crustal thinning is more extensive in the East Orphan Basin, whilst thinning in the West Orphan Basin resulted in crust of variable thickness from 5-15 km thick (beta factor 2-6) (Fig. 8h), which remains the case until 0 Ma (Fig. 6h). Overall, the level of crustal thinning in Model 6c is notably lower at 150 Ma, which continues to be the case until 0 Ma (long after the cessation of extension) compared to Models 6a, b and d.

In Model 6d, the location of the Flemish Cap at 200 Ma is identical to Model 6c, however, the Orphan Knoll is located much closer to the Flemish Cap than the North American necking zone (Fig. 4i). The result of this starting configuration is that by 150 Ma, significant crustal thinning in the East Orphan Basin has occurred, locally down to 5 km (beta factor 6) whilst retaining 15 km thick crust (beta factor 2) in some areas (Fig. 9i). By 100 Ma, crustal thinning in the East Orphan Basin results in widespread crust of < 10 km thick (beta factor <3), whilst in the West Orphan Basin the crustal thickness at this time is predicted to be generally 10-15 km (beta factor 2-3), but locally 5 km thick (beta factor approximately 6) (Fig. 8i). This scenario persists until 0 Ma (Fig. 6i & 12i), i.e. much more extensive thinning in the East than the West Orphan Basin.

Despite the major differences between the results of the models outlined above, some similarities persist across the predictions for crustal thickness and evolution in the Orphan Basin. In particular, in all models that include a separate plate for the Flemish Cap (Models 2, 3, 4, 5 and 6a-d), a region of thin crust in the southernmost East Orphan Basin (north of where the Flemish Cap joins the North American Necking zone; Fig. 1) is predicted. The extent and

geometry of this thin region varies slightly between models with this region being affected by more widespread thinning in some models (e.g., Models 6b and 6d).

Southern Grand Banks and Iberian Margin

Although the role of the Flemish Cap and its implications for the development of the Orphan Basin have been described above, this section focuses on the resultant deformation outboard (east) of the Flemish Cap and to the south on the Newfoundland and the conjugate Iberian margins, where again the Flemish Cap appears to have played an integral role. As with the results from some of the other areas described in this section, the modelled evolution of crustal deformation in this region can be considered to belong to one of multiple scenarios. These are: scenario 1 (marginal crustal thickness < 10 km at 0 Ma; Model 1), scenario 2 (marginal crustal thickness generally 10-15 km at 0 Ma; Models 2, 3, 4 and 5), scenario 3 (marginal crustal thickness 10-15 km and crust 25-30 km thick northeast of the Flemish Cap at 0 Ma; Model 6a and 6b), and scenario 4 (marginal crustal thickness 10-15 km and crust 20 km thick northeast of the Flemish Cap at 0 Ma; Model 6c and 6d).

In scenario 1, by 150 Ma, significant thinning of the crust on the Iberian Margin and Grand Banks is predicted to result in crust 10-20 km thick, decreasing towards the south (Fig. 9a), whereas in scenario 2 the crust is modelled to be typically 15-25 km thick, with less significant along margin variation (Fig. 9c-e). In scenario 3 however, rotation of the Flemish Cap is predicted to result in significant crustal thickening to > 50 km on the Galicia Bank and east of the Flemish Cap (Fig. 9f-g), whilst in scenario 4, this rotation is predicted to result in crust approximately 30-35 km thick east of the Flemish Cap (Fig. 9h-i).

By 100 Ma (Fig. 8), in scenario 1, most of the Iberian and Newfoundland margins are predicted to have had crustal thicknesses generally < 10 km thick, whereas in scenario 2, by 100 Ma, this area is predicted to have crustal thicknesses of approximately 15 km. In scenario 3, the crustal thickening that was apparent earlier at 150 Ma (Fig. 9f- g) caused by the rotation of the Flemish Cap is still apparent at 100 Ma (Fig. 8 f- g) compared to the models where such thickening did not occur. However, this region now has a crustal thickness of 15-25 km thick. Moreover, in scenario 4, the extent of the crustal thickening caused by the rotation of the Flemish Cap is again less significant at 100 Ma than for the scenario 3 models (Fig. 8h-i). In particular, a region of crust approximately 20-25 km thick remains east of the Flemish Cap and the crust of the northern Iberian margin (Fig. 8h-i) is slightly thicker than in the models from scenarios 2 and 3. For all scenarios, the crustal thicknesses at 100 Ma (Fig. 8) persist through the entirety of the post-breakup evolution (Fig. 7) to present (Fig. 6)

The Rockall-Hatton area

As with the Orphan Basin and the Porcupine Basin and Bank region, the Rockall-Hatton area represents one of the regions with highly variable results between models but for which resultant crustal thicknesses can be considered to belong to different scenarios, for ease of description. These are: scenario 1 (crustal thickness of 20-25 km at 0 Ma; Model 1), scenario 2 (crustal thicknesses of approximately 15 km northwest, 5-15 km southwest and 20 km southeast of Rockall-Hatton Bank at 0 Ma; Models 2, 3 and 4), scenario 3 (crustal thicknesses of generally 15-20 km at 0 Ma; Model 5), and scenario 4 (highly variable crustal thicknesses

of 5-20 km thick southeast of Rockall-Hatton Bank and 20 km to the northwest at 0 Ma; Models 6a-d). In addition, there are some minor variations between the results for the Rockall-Hatton area in Model 6a and the other constituents of scenario 4, expanded upon below.

In scenario 1 at 150 Ma, widespread diffuse thinning, as it is not spatially restricted as Model 1, does not include a separate Hatton-Rockall Bank micro-continental fragment (Fig. 4a) to focus deformation into smaller areas such as the Rockall Basin (Fig. 9a). This scenario results in crust around 25 km thick (beta factor < 1) for Model 1 at 150 Ma. In scenario 2 at 150 Ma, thinning is apparent in the Rockall Basin where crustal thicknesses from 20-25 km (beta factor < 1) are widespread and are locally as low as 15 km (beta factor 2) (Fig. 9a, c & d), whilst no thinning is yet predicted to the northwest of the Rockall-Hatton Bank micro-continental fragment. In scenario 3, crustal thickness at 150 Ma is similar to that of scenario 1 in that the absence of a separate Hatton-Rockall Bank micro-continental fragment results in widespread diffuse thinning typically resulting in crustal thicknesses of 20-25 km (beta factor <1) (Fig. 9e). In scenario 4 at 150 Ma (Fig. 9f-i) in the Rockall Basin (Fig. 1), much greater localisation of thinning is predicted compared to the other scenarios considered. In particular, in scenario 4, crustal thicknesses of <10 km are predicted, whilst in other parts of the Rockall Basin local crustal thicknesses of 15-25 km (beta factor <1-2) are predicted. Moreover, at 150 Ma in scenario 4 in the region to the northwest of the Rockall-Hatton Bank micro-continental fragment (i.e. the southeast Greenland Margin), crustal thickening is predicted, which is described in the following section dedicated to the southeast Greenland margin.

At 100 Ma, all scenarios (1-4) produce a similar distribution of crustal thicknesses to those of 150 Ma except that the crust is generally predicted to be thinner (Fig. 8). For example, in scenario 1 at 100 Ma, crustal thickness is around 20 km (beta factor <1), compared to 25 km thick at 150 Ma. Similarly, scenario 2 at 100 Ma predicts crustal thicknesses around 15-20 km, compared to 20-25 km thick at 150 Ma, and scenario 4 at 100 Ma predicts crustal thicknesses of 10-20 km thick, compared to 15-25 km for 150 Ma. Finally, as with the 150 Ma results, the Rockall-Hatton Bank area in scenario 3 is near identical to that of scenario 1 for 100 Ma.

At 50 Ma (Fig. 7), the crustal thickness in the Rockall Basin is generally similar to the 100 Ma results (Fig. 8), and as with most regions described in this result section the crustal thicknesses predicted at 50 Ma closely resemble those at 0 Ma (Fig. 6) for all scenarios.

Labrador Sea and southeast Greenland

Model input parameters for the Labrador Sea and southeast Greenland were not varied between models as much as for other locations in the study area as these proximal regions did not represent the primary focus of this study. Variation in model results in these regions is entirely controlled by changing input parameters elsewhere in the modelled domain. Despite this, predictions of crustal thickness for these regions do vary between model results.

On the margins of the Labrador Sea, modelled deformation is near identical in all models, and any minor variations are likely caused by varying parameters (e.g., poles of rotation) elsewhere in the modelled domain (Table 1). This is the case for both the final result (0 Ma; Fig. 6) and the evolution from 200 Ma to this point (Figs. 7-9). Moreover, in Model 1, when the global parameters are used (Müller et al., 2016; Matthews et al., 2016) compared to those of

Nirrengarten et al. (2018), the only observable difference from the results obtained in Models 2-6d is that global constraints do not predict an area of anomalously thin crust on the northern Labrador margin. Overall, at 0 Ma (Fig. 4), all models predict crustal thickness on the margins of the Labrador Sea around 15 km thick (beta factor of approximately 2) with some localised thinning of < 10 km (beta factor of approximately <3) with the temporal evolution to reach this point not varying significantly between models.

Despite not being the focus of this study, results for southeast Greenland show more variation between models than those of the Labrador Sea (Fig. 6). The reason for this is that inputs for the conjugate Rockall-Hatton area are intentionally varied considerably between models (Fig. 4), which impacts the southeast Greenland margin. First, considering the modelled crustal thickness at 0 Ma, it can be seen that in Model 1, using the global constraints (Müller et al., 2016; Matthews et al., 2016), results in slightly thicker crust (approximately 20 km) in southeast Greenland for more of the margin (particularly to the south) than for Models 2-5. In Models 6a-d however, when a closer fit between the Rockall-Hatton Bank and the Irish Margin is used (Fig. 4f-i) compared to Models 2-5, a thicker modelled crust at 0 Ma is predicted, particularly to the north of the southeast Greenland margin. The development of this slightly thicker crust on the southeast Greenland margin when a closer fit between the Rockall-Hatton Bank and the Irish margin is modelled is particularly apparent at 100 Ma (Fig. 8f-i) and 150 Ma (Fig. 9f-i).

Bay of Biscay

Results for the Bay of Biscay are not as variable as for other modelled regions discussed in this study as this region did not represent the focus of this study in the same way that the Orphan Basin and Irish margin did. In all models, by 0 Ma, significant crustal thickening in the easternmost Bay of Biscay is predicted (Fig. 6). This is more apparent in Model 1 as the continental margins are wider making the thicker region more extensive in area (Fig. 6). In all models, crustal thickness in the Bay of Biscay increases from around 15 km (beta factor 2) in the west to > 50 km (beta factor 0) in the east.

Discussion

Comparison between deformable model results and regional observations

In this section, the results of the GPlates deformable models (Figs. 6-14) are compared to geological and geophysical observations from across the modelled region, principally the gravity inversion results from Welford et al. (2012) (Fig. 15) but also other observations such as the interpretation of seismic reflection data (e.g., Yang, 2012; Keen et al., 2014; Gouiza et al., 2016). This was undertaken to test whether the various models accurately reproduced deformation of the margins of the southern North Atlantic. The gravity inversion in Welford et al. (2012) utilised the GRAV3D inversion algorithm (Li and Oldenburg, 1996; Li and Oldenburg, 1998), which is also applied in Welford et al. (2010, 2018).

The inputs for deformable models that result in features shared with real, independent observations at 0 Ma can be deemed to be candidates for attributes that may have influenced the regional evolution. Furthermore, insights into which basins can be considered related are

also possible, and are described below. The results of the gravity inversion by Welford et al. (2012) are directly compared to the final results of Model 6c. Model 6c is chosen for this comparison as this result is the closest (of all the deformable model results) to the crustal thicknesses predicted by gravity inversion (Fig. 15).

Porcupine Bank and Basin

Previous work has shown that the Porcupine Basin has a complex rift and post-rift history (Jones et al., 2001; Reston et al., 2004; Naylor and Shannon, 2005; O'Reilly et al., 2006; Yang, 2012; Chen et al., 2018; Prada et al., 2018; Watremez et al., 2018). This complex rift history is depicted in the results of the deformable plate tectonic models, including the prediction of hyperextension.

Resultant crustal thicknesses derived through deformable models show general similarity with the predictions of gravity inversion (Fig. 15). However, crustal thickness, both in the Porcupine Basin and the Porcupine Bank, are largely over predicted in the models, which means beta factors are intrinsically under predicted. The crust in the Porcupine Basin has been documented to be locally as low as 2 km thick based on wide-angle seismic data (O'Reilly et al., 2006). This is possibly because stretching, and thus thinning, had already initiated by the Permian or Triassic (Štolfová and Shannon, 2009), or even as early as the Carboniferous (Tate, 1993). This means that there is inherited thinning that occurred prior to the start of the modelled interval from 200 – 0 Ma. However, given that the models are capable of producing reasonable first-order reconstructions of deformation, this may imply that tectonic and crustal thinning prior to the Jurassic was minor, or that the pre-cursory extension did not significantly alter the crustal structure, perhaps because geodynamic processes remained decoupled. In addition, Chen et al. (2018) proposed following the analysis of wide-angle seismic data that the Porcupine Basin represents a propagating rift with variations in strain along the rift axis, a situation that is reproduced in our models that include a rotation of the Porcupine Bank. This suggests that such a scenario proposed by Chen et al. (2018) was likely during the early evolution of the Porcupine Basin.

For the Porcupine Basin and Bank, Models 6a-d produced crustal thicknesses that were most comparable with those derived from gravity inversion (Welford et al., 2012) and the interpretation of wide-angle seismic data (O'Reilly et al., 2006). Models 6a-d all contain significant rotation of the Porcupine Bank (Tables 1 & 2a-d), implying that this phenomenon is required to explain the distribution of crustal thicknesses observed on the gravity inversion results. Moreover, Models 6a-d realistically reproduce the two crustal thin spots depicted in the gravity inversion. Regarding the two crustal thin spots, the Porcupine Basin can be divided into a northern and a southern region by the Clare Lineament (Tate, 1993). Although the models presented did not include any specific features to represent the Clare Lineament, the resultant crustal thickness maps for the Porcupine Basin in Models 6a-d show a division into northern and southern sub-basins. This perhaps implies that such a division may be a direct product of rifting, and in particular rotation of the Porcupine Bank, rather than as a result of such a discrete structure. In addition, more extensive stretching in the south of the Porcupine Basin than the north has been concluded by previous work (Watremez et al., 2018; Chen et al., 2018), which may be further evidence that rotation of the Porcupine Bank occurred. Overall, the results

suggest that significant clockwise rotation of the Porcupine Bank is required to account for the extensional deformation that resulted in the formation of the Porcupine Basin. Another possibility is that the Porcupine Bank and Basin are segmented, leading to greater extension in the south than the north. Geological and geophysical evidence for such segmentation has however not been recognised, and thus we prefer the rotation model.

One of the most enigmatic features of the Porcupine Basin remains the nature and origin of the Porcupine Median Ridge (e.g., Reston et al., 2004; Calvès et al., 2012). Although they do not provide conclusive evidence, the results presented do indicate that stretching may have been on the order capable of hyperextension (i.e. beta factors > 6; Fig. 13), and thus a mantle exhumation origin of the Porcupine Median Ridge is plausible at this location, but it does not allow us to rule out other explanations such as an igneous origin, as favoured by some workers (Calvès et al., 2012).

Orphan Basin and Flemish Cap

The Orphan Basin represents one of the areas for which the different deformable plate tectonic models produce different results (Figs. 12). This is as a result of this study focusing on the tectonic role and origin of the Orphan Knoll and Flemish Cap, which have proven to be integral to the formation of the Orphan Basin. Overall, the results of the models show general agreement with crustal thicknesses obtained from gravity inversion (Welford et al., 2012) (Fig. 15), with our preferred model again being Model 6c. In addition, the timing of deformation in the models is in general agreement with geological observations, suggesting that thinning may have begun earlier in the East than the West Orphan sub-basins (Gouiza et al., 2016) but that by the Jurassic, rifting was documented across the Orphan Basin (Dafoe et al., 2017).

As significant internal deformation within the Flemish Cap is not documented by geological and geophysical observations (Funck, 2003; Sibuet et al., 2007), we interpret this to be strong evidence for the clockwise rotation of the Flemish Cap from a more northern position, as proposed in Sibuet et al. (2007) and modelled in Models 2-6d. Models that do not include rotation of the Flemish Cap and Orphan Knoll (Model 1) do not result in sufficient thinning of the crust in the Orphan Basin. When no rotation of the Flemish Cap is included, there is an overlap at 200 Ma between the Flemish Cap and the Iberian margin necking zone (Fig. 4a). The model that appears to reproduce the present-day structure of the Orphan Basin most closely is Model 6c, but localised aspects of all models that include a rotating Flemish Cap can be seen to resemble the results obtained from gravity inversion. For example, for all models that include a rotation component for the Flemish Cap, a region of thin crust can be observed to the south of the westernmost Flemish Cap micro-continental fragment, whilst a comparable crustal thin-spot is also intriguingly documented on the results of the gravity inversion, perhaps a local manifestation of thinning due to rotation (Fig. 15).

Despite the significance and necessity of Flemish Cap rotation, its rotation in Models 6a and 6b results in unrealistic deformation of Galicia Bank on the Iberian margin. This implies that although rotation of the Flemish Cap is very likely required to explain the observed crustal geometries of the Orphan Basin (as outlined above), perhaps the rotation is unlikely to be as extensive or substantial as the scenarios modelled in Models 6a and 6b. Thus, constraints on

737 the amount of rotation that the Flemish Cap may have undergone can be obtained, i.e. rotation
738 of the Flemish Cap is more likely to be comparable to the situation considered in Models 6c
739 and 6d. Overall, the results of the deformable models suggest that rotation of the Flemish Cap
740 was of comparable magnitude to that proposed in Sibuet et al. (2007) (i.e. it moved 200-300
741 km southeast and rotated approximately 43° with respect to Galicia Bank and Iberia).

742 In addition to providing insights into the evolution of the Flemish Cap, the results allow us to
743 make inferences regarding the origin of the Orphan Knoll. For example, in models that do not
744 include a separate Orphan Knoll micro-continental fragment, the structural division (thicker
745 crust of approximately 15-20 km) observed between the East and West Orphan sub-basins in
746 the gravity inversion results (Fig. 15e) is not retained (Fig. 12a, d & e). Moreover, this structural
747 division is also observed from seismic data, which depict a thinned crust (4–16 km thick)
748 underneath the eastern and western parts of the Orphan Basin, forming two sub-basins
749 separated by a wide structural high with a relatively thick crust (17 km thick) (Gouiza et al.,
750 2016). This implies that the preservation of some thicker crust at this location during rifting
751 was likely.

752 However, as different geometries for the Orphan Knoll were considered, the model results
753 allow us to also comment upon this aspect. In particular, when the larger, more elongate
754 geometry (as proposed in Nirrengarten et al. 2018 and modelled in Model 2) was used, a
755 significant structural division between the East and West Orphan sub-basins results in the
756 prediction of greater crustal thicknesses in the central region compared to the predictions of
757 gravity inversion. When a smaller geometry for the Orphan Knoll was used (defined using
758 seismic basement; Fig. 2), this produces overall crustal thicknesses that are more comparable
759 to those from gravity inversion. However, this does not produce such a clear division between
760 the East and West Orphan sub-basins. Therefore, a singular, relatively undeformed, micro-
761 continental fragment in the region of the Nirrengarten et al. (2018) Orphan Knoll seems
762 unlikely. Rather this region may be occupied by multiple, smaller continental crustal fragments
763 that have undergone less deformation than crust in the adjacent East and West Orphan basins.
764 Alternatively, this may be explained by the processes of depth-dependent stretching, which has
765 been proposed in previous works analysing the crustal architecture of the Orphan Basin. Gouiza
766 et al. (2016), for example, proposed a large discrepancy between brittle extension localized in
767 the upper crust and the overall crustal thinning. A limitation of our deformable models is that
768 they do not include depth dependant stretching (Gurnis et al., 2018). This may explain some of
769 the local observations from the gravity inversion results. Alternatively, the simplification of
770 the deformable domain used in these models does not properly address the localisation of
771 spatially and temporally discrete rifting phases that may be overlapping in the Jurassic and
772 Cretaceous rift events (e.g., Naylor and Shannon, 2005).

773 In addition to the geometry of the Orphan Knoll, its position at 200 Ma, and its trajectory
774 thereafter have been shown to have a significant influence on resultant crustal deformation
775 (Models 6a-d). The results of the deformable models indicate that the most likely position of
776 the Orphan Knoll at 200 Ma is near equidistant between the necking zone of the Flemish Cap
777 and the North American margin necking zone, as this situation (Model 6c) produces a
778 distribution of crustal thicknesses at 0 Ma that is most comparable to the results of the gravity
779 inversion (Fig. 15).

Overall, according to the results of the deformable models, to explain the crustal evolution and deformation of the Orphan Basin, relatively undeformed Orphan Knoll and Flemish Cap micro-continental fragments are required. As such, the preferred model for the evolution of the Orphan Basin is Model 6c. However, it seems plausible that some internal deformation within these blocks would provide a stronger agreement between the independent results of the deformable models and the gravity inversion, a situation that the modelling setup used in this study (Gurnis et al., 2018) unfortunately does not allow for.

Southern Grand Banks and Iberian Margin

The southern Grand Banks (i.e. south of the Flemish Cap) and the conjugate Iberian margin represent the only area modelled in this study where the use of the global constraints produced deformation more akin to observations. In particular, Model 1 used the Müller et al. (2016) continent ocean boundaries (COBs) to define the ocean-ward limit of continental crust, whereas Models 2-6(a-d) used the edge of continental crust (ECC) from Nirrengarten et al. (2018). The Müller et al. (2016) COBs are taken from the global compilation and include exhumed mantle (hyper-extended) domains as material continent-ward of the COB (e.g., on the Grand Banks, offshore Newfoundland). Conversely, the Nirrengarten et al. (2018) ECC is defined locally in the southern North Atlantic and places the exhumed mantle domain ocean-ward of the ECC. The result of including the exhumed domains in global models is that beta factors more akin to hyper-extension are predicted by deformable Model 1 for this area.

As with the other areas considered during this work, there again appears to be more similarity with the beta factor map than with crustal thickness, perhaps again suggesting that thinning may have begun earlier than the modelled interval, that initial crustal thickness was less than 30 km, or that the mapping of the ECC or necking line was not accurate.

The Rockall-Hatton area

The geological evolution of the Rockall-Hatton area is well-acknowledged as being particularly enigmatic due to poor seismic and well control (Tate et al., 1999; Shannon et al., 1999; Schofield et al., 2018; Roberts et al., 2018). It is for this reason that in our models the region was included as a singular polygon (Nirrengarten et al., 2018), despite it being known that the region within the polygon contains numerous basins and structures that were active during rifting (Elliott and Parson, 2008). However, despite this acknowledged simplification, there are many ways in which the results of the deformable models are in general agreement with the predictions from the gravity inversion, given the limitations of each approach. For example crustal thicknesses in the Rockall Basin from deformable Models 6a-6d are of a similar magnitude to the values derived from gravity inversion (Fig. 15) and seismic data which show crust in the Rockall Basin to be around 10 km thick in parts (Shannon et al., 1999). It is for this reason that Models 6a-6d represent our preferred models for this region.

Labrador Sea margins and southeast Greenland

The margins of the Labrador Sea and southeast Greenland represent peripheral regions that did not form the focus of this work. Thus, in order to achieve optimal results for the regions of focus to the south, some unrealistic deformation may be predicted in some of the models of

these regions. In particular, structural inversion caused by the northward movement of the Rockall-Hatton Bank of the magnitude predicted in our Models 2, 3, 4 & 6a-d is likely to be unrealistic as such deformation is not documented in southeast Greenland. It is more likely that deformation was accommodated within the Rockall-Hatton Bank, which was modelled as a single rigid polygon (Fig. 4) despite this region containing multiple basins and structures that were known to be active during rifting (Hitchen, 2004; Elliott and Parson, 2008).

Bay of Biscay

On the margins of the Bay of Biscay, the models predict significant crustal thinning in the west (~10-15 km) and thickening to the east, where crustal thickness may exceed 40 km (Fig. 6). The unrealistic crustal thickening may indicate that the poles of rotation in this region require further modification. However, the Bay of Biscay was not the focus of this work, which as outlined previously focused on the Canadian and Irish margins. As such future work should seek to further constrain the tectonic history of this region, including the role of oblique extension and the poles of rotation for any micro-continental fragments.

Compression and inversion of the passive margins of the southern North Atlantic

Compression is indicated at numerous locations, in many of the results of the deformable models. For example, in proximity to the rotating micro-continental fragments it is common (e.g., east of Flemish Cap and west of Porcupine Bank; Models 6a-d at 150 Ma Fig. 9f-i). In addition, more significant thickening due to compression is predicted in the Pyrenean region in all models, which can be observed by 100 Ma (Fig. 8) and is retained until present (Fig. 6). This compression is to be expected in passive margin basins and adjacent regions (Cloetingh et al., 2008). Comparison with regional observations shows that these predictions are reasonable, as inversion of marginal basins is a commonly documented phenomena in the region (Doré et al., 1996; Tate et al., 1999; Yang, 2012; Cadenas et al., 2018; Druet et al., 2018).

For example, in the northern Porcupine Basin it has been demonstrated (using seismic reflection data) that Late Jurassic-Early Cretaceous compression likely occurred (Yang, 2012). In addition, more recent inversion is observed of Cenozoic age from across the European northeast Atlantic margin, including; domes, anticlines, reverse faults and broad-scale inversions (Doré et al., 1996; Doré et al., 2008). Our models predict the Late Jurassic-Early Cretaceous compression documented in the northern Porcupine Basin (Yang, 2012), and even allow us to suggest the cause of this deformation being the rotation of the Porcupine Bank. However, our models do not predict the more recent Cenozoic inversion as much of this occurs post-breakup, and through mechanisms that cannot be expressed through the GPlates deformable plates workflow (Gurnis et al., 2018), such as far-field orogenic stress or breakup/spreading forces such as ridge push (Doré et al., 2008).

Further south, on the Iberian margin, previous work also documents compression in the Bay of Biscay and Pyrenees region due to the kinematics of the Iberian Plate (Vissers and Meijer, 2012a; Vissers and Meijer, 2012b). Significant crustal thickening due to compression is predicted by our models of this region, in line with these regional observations. However, the kinematics of the Iberian plate, and thus the opening mechanism of the Bay of Biscay, remain

a subject of debate (Tavani et al., 2018). Therefore, although our models also predict this deformation, as we have not explicitly experimented with different opening scenarios for the Bay of Biscay we are not able to make significant inferences regarding the mechanisms involved.

The Newfoundland margin has also been found by previous work to exhibit evidence of compression compatible with observations in our models (Grant, 1987; Enachescu, 2006; Lau et al., 2006). Further north, on the Labrador Margin, Dickie et al. (2011) documented structural inversion on seismic data of Coniacian age, which is not predicted by our models. Moreover, structural inversion to the north of the present study area in the Davis Strait and Baffin Bay region is widespread (Oakey and Chalmers, 2012; Gion et al., 2017; Peace et al., 2018c). Although, our modelled domain does not extend to these latter regions these observations demonstrate that marginal compression is a widespread and significant event across the North Atlantic region.

Summary of comparison between modelling results and observations

Overall, the deformable plate tectonic models presented have reproduced deformation at 0 Ma that is in many ways comparable to observations made on the margins of the southern North Atlantic, given the limitations of the regional geological understanding and modelling approach. In particular, Model 6c appears to produce crustal thickness values comparable to those derived from gravity inversion for more regions than the other models. Thus, we deem Model 6c to be the best reconstruction of micro-continental fragments of all models presented herein. However, even within the results of this best approximation model, several regions still depict discrepancies from regional geological and geophysical observations. In particular, such areas include: the margins of the Bay of Biscay, southeast Greenland and the Rockall-Hatton Bank area.

Implications for conjugate margin studies

It is well-acknowledged and documented that in order to fully comprehend rift evolution, and thus the large-scale processes driving deformation, both conjugate margins must be studied (Lister et al., 1986; Chian et al., 1995; Welford et al., 2012; Ball et al., 2013; Louden et al., 2013; Gernigon et al., 2015; Peace et al., 2016). However, the inclusion of rotating, independent, micro-continental fragments within the rift (as examined in this study) has profound implications for conjugate margin studies (Sibuet et al., 2007; Nirrengarten et al., 2018). The reason for this is that margin segments that today look as if they are conjugate did not originally form as conjugates. In fact they are pseudo-conjugates that have been translated into locations with orientations that appear conjugate due to poly-phase rifting and the formation and subsequent rotation of micro-continental blocks. This is particularly true for micro-continental blocks that have undergone a significant rotation or along margin movement such as the Flemish Cap (Sibuet et al., 2007). Regarding the Flemish Cap, in our preferred model (Model 6c), we interpret that the northeastern Flemish Cap was conjugate to the Porcupine Bank, whilst the southwest Flemish Cap was conjugate to the Goban Spur and Galicia Bank (Fig. 4h). Thus, some ‘conjugate margin’ studies may be overly simplistic in areas such as the southern North Atlantic where multiple, disparate continental fragments may

have originally been part of the same rift system. The situation can be further complicated in areas such as this area which contain triple junctions (i.e. extinct Labrador Sea spreading axis joining the main North Atlantic axis; e.g., Srivastava, 1978), in addition to rift axes that failed to achieve breakup e.g., Rockall Basin (Joppen and White, 1990).

An example of this type of ambiguity in the studied region is determining which parts of the East and West Orphan basins on the Canadian Margin can be considered conjugate to the Porcupine or Rockall Basins on the Irish Margin (Skogseid, 2010). Some previous reconstructions place East Orphan Basin conjugate to Porcupine Basin and West Orphan Basin conjugate to Rockall Basin. However, according to the reconstruction of Nirrengarten et al. (2018), as used in the models described, the Rockall Basin may not be conjugate to West Orphan and, furthermore, the Rockall Basin might be more akin to East Orphan and the Porcupine Basin may not be conjugate to either the West or East Orphan basins. Overall, due to the complications of determining precisely which basins and margin segments were conjugate in the rift, we suggest describing candidate basins as connected basins rather than conjugate margins or basins. Future work should seek to determine which, if any, of the Irish and Eastern Canadian offshore basins can be considered connected or related.

Implications for local and regional magmatic evolution

The interplay between extensional tectonic processes and magmatism represents one of the most studied and debated topics within the Earth sciences (White and McKenzie, 1989; White, 1992; Foulger and Anderson, 2005; Larsen et al., 2009; Foulger et al., 2015; Peace et al., 2016; Peace et al., 2017a; Petersen et al., 2018; Clarke and Beutel, 2019). The results of the models presented herein allow us to compare predictions of the timing and extent of significant crustal deformation with dated occurrences of igneous rocks (e.g., Hansen et al., 2009; Keen et al., 2014; Wilkinson et al., 2016; Á Horni et al., 2017). Thus, they allow us to test the potential role of plate tectonic processes in the development of rift-related magmatism. However, without careful consideration of the model input parameters, they do not allow us to discern between different mechanisms, i.e. the difference between active and passive rifting (e.g., Geoffroy, 2005; Franke, 2013; Geoffroy et al., 2015). In addition, there are factors that may also exert some control on magmatism such as inherited mantle fertility or re-fertilization as necking and exhumation processes evolve (e.g., Picazo et al., 2016) and also potential temperatures (Nielsen, 2002), that our models do not allow us to comment upon directly.

Charlie-Gibbs Volcanic Province

The Charlie-Gibbs Volcanic Province (CGVP) is a magmatic province documented from seismic data in the northern West Orphan Basin, near the western termination of the Charlie-Gibbs Fracture Zone (CGFZ) (Pe-Piper et al., 2013; Keen et al., 2014). The CGVP comprises a suite of seamounts and flows (Keen et al., 2014), and can be considered as part of a sequence of Mesozoic-Cenozoic rift-related magmatism on the Newfoundland Margin (Pe-Piper et al., 1992; Pe-Piper et al., 2007; Peace et al., 2018c). Keen et al. (2014) stratigraphically dated the CGVP as Mid-Late Cretaceous, and postulated that the emplacement of these magmatic rocks may have been related to transtensional movements on the CGFZ, i.e. a significant kinematic, plate tectonic control on magmatism. However, although a Late Cretaceous age is credible in

943 the regional geological context, it should be considered approximate due to the sparse well
944 control in the northern West Orphan Basin.

945 The deformable results show that in models where a separate plate is included for the Orphan
946 Knoll, there is a rapid thinning of the crust, and therefore high beta factors, at the location of
947 the CGVP during the interval ca. 80 – 120 Ma (Figs. 7-10, and 15), i.e. at a similar time to the
948 emplacement of the CGVP (Keen et al., 2014). Thus, it appears that the modelling results
949 provide evidence in support of the formation mechanism proposed by Keen et al. (2014).
950 Moreover, the results indicate that the Orphan Knoll is integral to the evolution of the Orphan
951 Basin and surrounding area, and further justify its inclusion as a separate plate in models (i.e.
952 Nirrengarten et al., 2018).

953 The results of the models herein are intriguingly similar to the predictions of the numerical
954 models by Beutel (2005) who also predicted stress concentrations at ridge-transform-
955 intersections that could result in adiabatic melting and thus seamount formation. In addition,
956 the numerical modelling of Ammann et al. (2017) suggests that rift obliquity plays a significant
957 role in the formation of large oceanic fracture zones such as the CGFZ, potentially providing
958 further evidence that the CGFZ underwent significant oblique extension. Finally, given that
959 oceanic transforms have been suggested to form at the locations of major pre-existing
960 structures, a link between tectonic and magmatic processes seems plausible, with such barriers
961 to rifting being associated with magmatism elsewhere in both numerical models (Koopmann
962 et al., 2014) and geological observations (Peace et al., 2017a).

963 Finally, however, many other factors are known to influence magmatism. Such factors include
964 mantle fertility (Foulger et al., 2005; Foulger and Anderson, 2005; Shorttle et al., 2014; Picazo
965 et al., 2016), and also possibly thermal anomalies (White and McKenzie, 1989; Geldmacher et
966 al., 2005), neither of which can be ruled out as either dominant or complementary factors based
967 on the model results.

968 ***Limitations of the GPlates deformable models methodology***

969 Here, we have applied the GPlates deformable modelling methodology described in Gurnis et
970 al. (2018) to the passive margins and rift basins of the southern North Atlantic region (Fig. 1).
971 Whilst comparison of our results with other, independent predictions of crustal thickness and
972 structure shows general, large-scale similarity, there remain disparities that can be largely
973 explained due to the limitations of this methodology. However, through recognition of the
974 limitations of the methodology, we are able to discern the most important aspects of the
975 kinematic evolution of the North Atlantic, including the potential controlling mechanisms.

976 First, the methodology utilised herein requires the assumption that at the start of the model, the
977 crust is homogeneous and of uniform thickness. However, even if the models were capable of
978 starting with a heterogeneous crust of variable thickness, realistically predicting such
979 parameters (e.g., thickness, strength, pre-existing heterogeneity) would likely prove
980 problematic, and possibly introduce further uncertainties.

981 In addition, starting the models at 200 Ma likely also influenced the final results. The reason
982 for this is that regional stretching, or even rifting, likely occurred prior to 200 Ma (Stoker et

al., 2016). This means that the crustal thickness at 200 Ma was likely highly variable, which is not accounted for in the models. However, given that comparable results, given this limitation are produced, this perhaps implies that crustal thinning prior to 200 Ma was insignificant at the scale considered in this work.

Another assumption of the modelling approach that is likely to have had an impact upon the results is that the model setup requires the boundaries to the deformable domain to be 'hard', i.e., deformation cannot diffuse into the surrounding undeformed continent, and overlapping rift events cannot be modelled, which has been shown to be the case in the region (e.g., Porcupine Basin - Bulois et al., 2018). This means that domains of the model have to be selected to be either deformable or non-deformable, i.e. one cannot define regions that are only deformable for part of the modelled interval. The result of this is that it is not possible to implement a scenario in which a particular domain, for example a microcontinental fragment, undergoes some thinning but not as much as surrounding regions. Moreover, another aspect of the hard model boundaries is that they may have introduced edge effects. Although the influence of edge effects appears to be relatively minor, edge effects may be influential in areas of oblique extension (such as the Pyrenees). Of all model limitations, the results presented herein suggest that the hard model boundaries may have had the most significant influence upon resultant crustal thicknesses, and thus calculated beta factors.

The initial location, geometry of the model inputs (Fig. 4), as well as the subsequent trajectory as determined by the poles of rotation (Tables 1-2a-d) influence the results. This is demonstrated through the highly variable results produced in Models 1-6c, which use different inputs. It is not only plausible, but likely, that some of the discrepancies between model results and real-world observations can be explained due to ambiguity in the model inputs. Our results presented herein (as well as preliminary experiments also conducted) suggest that of particular importance is the reconstructed position of the ECC as well as the timing of breakup. Future work should focus on better constraining these aspects to build on the models presented herein.

Another consideration is that as with other areas considered, the Rockall Basin likely underwent depth dependant differential stretching (Shannon et al., 1999) and our models, based on Gurnis et al. (2018), do not account for this. In particular, it is claimed that in the Rockall Basin, the upper crust has been thinned by a stretching factor of 8-10 while the middle and lower crust (and probably also the lithospheric mantle) were stretched by a factor of 2-3 (Shannon et al., 1999). This could explain some of the discrepancies between the deformable model results and the predictions of crustal thickness obtained from gravity inversion, although the more dominant influence upon the results is likely to be the lack of internal deformation within the modelled Rockall-Hatton Bank polygon, where rifting is documented (Hitchen, 2004; Elliott and Parson, 2008).

Finally, the assumption of symmetrical, depth-uniform, pure-shear deformation is likely to have also had an influence upon the final model results. For example, previous work has proposed that simple shear-type deformation may have been dominant in the Porcupine Basin (Reston et al., 2001; O'Reilly et al., 2006) and Labrador Sea (Peace et al., 2016), where observations of asymmetric basin fill and crustal geometry as well as detachments have been reported. However, despite the outlined simplification of the models, the application of pure

shear, symmetric, depth uniform thinning does appear to successfully manage to replicate the first-order crustal structure, and thus allows for differentiation between the geodynamic scenarios modelled (Fig. 4). This perhaps implies that at the scale considered in this study, rifting can be assumed to approximate pure shear-type deformation (e.g., McKenzie, 1978).

Conclusions

A suite of deformable plate tectonic models based on published constraints for the southern North Atlantic has been created in GPlates. The purpose was to test the viability of the GPlates deformable modelling approach, the published model inputs, and the influence of various pre-rift configurations. The conclusions of this study are as follows:

1) The GPlates deformable modelling tool has proven to be an effective means of testing different scenarios for the tectonic development of the southern North Atlantic.

2) Inclusion of micro-continental fragments, and more locally defined limits of continental crust, in deformable models, generally produces results more akin to observations, with the exception of the Grand Banks where global models produce more realistic deformation. This is likely due to the inclusion of the hyper-extended domains (coupled and exhumed) as continental material in such global models.

3) New poles of rotation for the Porcupine Bank, Orphan Koll, Flemish Cap and the Rockall-Hatton Bank produce deformation more akin to geological and geophysical observations.

4) Rotation of the Flemish Cap is unequivocally required to provide a geologically reasonable fit between North America and Iberia, with the paleo-position of the Flemish Cap in the proto-Orphan Basin producing reasonable estimates of crustal deformation given modelling limitations.

5) A smaller, refined geometry of the Orphan Knoll (after Nirrengarten et al. 2018) is probably more representative. However, this produces some unrealistic predictions for the crustal evolution of the Orphan Basin and thus smaller continental fragments may exist in the vicinity of the Nirrengarten et al. (2018) Orphan Knoll polygon.

6) Inclusion of the Orphan Knoll in models results in higher modelled beta factors in the northern West Orphan Basin near the termination of the CGFZ, and the site of the CGVP. Thus, we infer that the CGVP was potentially influenced by plate tectonic processes, with the Orphan Knoll probably being related.

7) The East and West Orphan basins formed separately due to the respective rotations of the Flemish Cap and the Orphan Knoll, which was likely associated with other continental fragments that subsequently contributed to the formation of the region of thicker crust between the East and West Orphan basins.

8) Basins that were considered to be conjugate, and thus strongly related, may in fact only have been brought into positions that appear to be conjugate through later rotation of micro-continental blocks, and thus their genesis is not as related as previously inferred.

Acknowledgements

Alexander L. Peace's postdoctoral fellowship at Memorial University of Newfoundland was funded by the Hibernia Project Geophysics Support Fund and Innovate NL. We would like to thank the GPlates development and maintenance team and the members of the MAGRiT group at Memorial University of Newfoundland for valuable scientific discussions. We would also like to acknowledge TGS for the generous provision of the seismic reflection data from the Orphan Basin. To prevent visual distortion of the data, most figures in this manuscript use perceptually uniform colour palettes from the Scientific Colour Maps collection for which we acknowledge Crameri (2018). Finally, we would like to thank the two anonymous reviewers for their constructive comments that greatly helped to improve this manuscript.

References

Á Horni, J., Hopper, J.R., Blischke, A., Geisler, W.H., Stewart, M., McDermott, K., Judge, M., Erlendsson, Ö., and Árting, U., 2017, Regional distribution of volcanism within the North Atlantic Igneous Province: Geological Society, London, Special Publications, v. 447, no. August, p. SP447.18, doi: 10.1144/SP447.18.

Ady, B.E., and Whittaker, R.C., 2018, Examining the influence of tectonic inheritance on the evolution of the North Atlantic using a palinspastic deformable plate reconstruction: , doi: 10.1144/SP470.9.

Alves, T.M., Bell, R.E., Jackson, C.A.L., and Minshull, T.A., 2014, Deep-water continental margins: Geological and economic frontiers: Basin Research, v. 26, no. 1, p. 3–9, doi: 10.1111/bre.12053.

Alves, T.M., and Cunha, T.A., 2018, A phase of transient subsidence, sediment bypass and deposition of regressive–transgressive cycles during the breakup of Iberia and Newfoundland: Earth and Planetary Science Letters, v. 484, p. 168–183.

Ammann, N., Liao, J., Gerya, T., and Ball, P., 2017, Oblique continental rifting and long transform fault formation based on 3D thermomechanical numerical modeling: Tectonophysics, doi: 10.1016/j.tecto.2017.08.015.

Archer, S.G., Bergman, S.C., Iliffe, J., Murphy, C.M., and Thornton, M., 2005, Palaeogene igneous rocks reveal new insights into the geodynamic evolution and petroleum potential of the Rockall Trough, NE Atlantic Margin: Basin Research, v. 17, no. 1, p. 171–201, doi: 10.1111/j.1365-2117.2005.00260.x.

Ashby, D., 2013, Influences on continental margin development: a case study from the Santos Basin, South-eastern Brazil: Durham University E-Theses,.

Van Avendonk, H.J.A., Lavier, L.L., Shillington, D.J., and Manatschal, G., 2009, Extension of continental crust at the margin of the eastern Grand Banks, Newfoundland: Tectonophysics, v. 468, no. 1–4, p. 131–148, doi: 10.1016/j.tecto.2008.05.030.

Ball, P., Eagles, G., Ebinger, C., McClay, K., and Totterdell, J., 2013, The spatial and temporal evolution of strain during the separation of Australia and Antarctica: Geochemistry, Geophysics, Geosystems, v. 14, no. 8, p. 2771–2799, doi: 10.1002/ggge.20160.

Barnett-Moore, N., Müller, R.D., Williams, S., Skogseid, J., and Seton, M., 2018, A reconstruction of the North Atlantic since the earliest Jurassic: Basin Research, v. 30, p. 160–185, doi: 10.1111/bre.12214.

Beniest, A., Koptev, A., Leroy, S., Sassi, W., and Guichet, X., 2017, Two-branch break-up systems by a single mantle plume: Insights from numerical modeling: Geophysical Research Letters, doi: 10.1002/2017GL074866.

Beutel, E.K., 2005, Stress-induced seamount formation at ridge-transform intersections: Geological Society of America Special Papers, v. 2388, no. 34, p. 581–593, doi: 10.1130/2005.2388(34).

Blischke, A., Arnarson, T.S., and Gunnarsson, K., 2011, The Structural History of the Jan

1114 Mayen Micro-Continent (JMMC) and Its Role During the Rift " J ump " Between the
1115 Aegir to the Kolbeinsey Ridge *, *in* AAPG, 3P Arctic-The Polar Petroleum Potential
1116 Conference & Exhibition, extended Abstract, Halifax, Nova Scotia, Canada,.

1117 Bullard, E., Everett, J.E., and Smith, A.G., 1965, The Fit of the Continents around the
1118 Atlantic: Philosophical Transactions of the Royal Society A: Mathematical, Physical and
1119 Engineering Sciences, v. 258, no. 1088, p. 41–51, doi: 10.1098/rsta.1965.0020.

1120 Bulois, C., Pubellier, M., Chamot-Rooke, N., and Watremez, L., 2018, From orogenic
1121 collapse to rifting: A case study of the northern Porcupine Basin, offshore Ireland:
1122 Journal of Structural Geology, v. 114, p. 139–162.

1123 Cadenas, P., Fernández-Viejo, G., Pulgar, J.A., Tugend, J., Manatschal, G., and Minshull,
1124 T.A., 2018, Constraints Imposed by Rift Inheritance on the Compressional Reactivation
1125 of a Hyperextended Margin: Mapping Rift Domains in the North Iberian Margin and in
1126 the Cantabrian Mountains: Tectonics, v. 37, no. 3, p. 758–785, doi:
1127 10.1002/2016TC004454.

1128 Calvès, G., Torvela, T., Huuse, M., and Dinkleman, M.G., 2012, New evidence for the origin
1129 of the Porcupine Median Volcanic Ridge: Early Cretaceous volcanism in the Porcupine
1130 Basin, Atlantic margin of Ireland: Geochemistry, Geophysics, Geosystems, v. 13, no. 6,
1131 p. 1–18, doi: 10.1029/2011GC003852.

1132 Chen, C., Watremez, L., Prada, M., Minshull, T., Edwards, R., O'Reilly, B., Reston, T.,
1133 Wagner, G., Gaw, V., Klaschen, D., and Shannon, P., 2018, From Continental
1134 Hyperextension to Seafloor Spreading: New Insights on the Porcupine Basin from
1135 Wide-angle Seismic Data: Journal of Geophysical Research: Solid Earth, doi:
1136 10.1029/2018JB016375.

1137 Chian, D., Keen, C., Reid, I., and Louden, K.E., 1995, Evolution of nonvolcanic rifted
1138 margins: new results from the conjugate margins of the Labrador Sea: Geology, v. 23,
1139 no. 7, p. 589–592, doi: 10.1130/0091-7613(1995)023<0589:EONRMN>2.3.CO;2.

1140 Clarke, D.B., and Beutel, E.K., 2019, Davis Strait Paleocene Picrites: Products of a Plume or
1141 Plates? Earth-Science Reviews, doi: 10.1016/j.earscirev.2019.01.012.

1142 Cloetingh, S., Beekman, F., Ziegler, P.A., van Wees, J.-D., and Sokoutis, D., 2008, Post-rift
1143 compressional reactivation potential of passive margins and extensional basins:
1144 Geological Society, London, Special Publications, v. 306, no. 1, p. 27–70, doi:
1145 10.1144/sp306.2.

1146 Crameri, F., 2018, Geodynamic diagnostics, scientific visualisation and StagLab 3.0:
1147 Geoscientific Model Development, v. 11, no. 6, p. 2541–2562, doi: 10.5194/gmd-11-
1148 2541-2018.

1149 Dafoe, L.T., Keen, C.E., Dickie, K., and Williams, G.L., 2017, Regional stratigraphy and
1150 subsidence of Orphan Basin near the time of breakup and implications for rifting
1151 processes: Basin Research, v. 29, p. 233–254, doi: 10.1111/bre.12147.

1152 Deemer, S., Hurich, C., and Hall, J., 2010, Post-rift flood-basalt-like volcanism on the
1153 Newfoundland Basin nonvolcanic margin: The U event mapped with spectral
1154 decomposition: Tectonophysics, v. 494, no. 1–2, p. 1–16, doi:
1155 10.1016/j.tecto.2010.07.019.

1156 Dickie, K., Keen, C.E., Williams, G.L., and Dehler, S.A., 2011, Tectonostratigraphic
1157 evolution of the labrador margin, atlantic canada: Marine and Petroleum Geology, v. 28,
1158 no. 9, p. 1663–1675, doi: 10.1016/j.marpetgeo.2011.05.009.

1159 Doré, A.G., Lundin, E.R., Doré, A.G., and Lundin, E.R., 1996, Cenozoic compressional
1160 structures on the NE Atlantic margin; nature, origin and potential significance for
1161 hydrocarbon exploration: Petroleum Geoscience, v. 2, no. 4, p. 299–311, doi:
1162 10.1144/petgeo.2.4.299.

1163 Doré, A.G., Lundin, E.R., Jensen, L.N., Birkeland, Ø., Eliassen, P.E., and Fichler, C., 1999,
1164 Principal tectonic events in the evolution of the northwest European Atlantic margin:
1165 Petroleum Geology of Northwest Europe: Proceedings of the 5th Conference, v. 5, p.
1166 41–61, doi: 10.1144/0050041.

1167 Doré, A.G., Lundin, E.R., Kusznir, N.J., and Pascal, C., 2008, Potential mechanisms for the
1168 genesis of Cenozoic domal structures on the NE Atlantic margin: pros, cons and some
1169 new ideas: Geological Society, London, Special Publications, v. 306, no. 1, p. 1–26, doi:
1170 10.1144/SP306.1.

1171 Druet, M., Muñoz-Martín, A., Granja-Bruña, J.L., Carbó-Gorosabel, A., Acosta, J., Llanes,
1172 P., and Ercilla, G., 2018, Crustal structure and continent-ocean boundary along the
1173 Galicia continental margin (NW Iberia): insights from combined gravity and seismic
1174 interpretation: Tectonics, v. 37, no. 5, p. 1576–1604.

1175 Dunbar, J.A., and Sawyer, D.S., 1989, Patterns of continental extension along the conjugate
1176 margins of the central and North ATLANTIC Oceans and Labrador Sea: Tectonics, v. 8,
1177 no. 5, p. 1059–1077, doi: 10.1029/TC008i005p01059.

1178 Eddy, M.P., Jagoutz, O., and Ibañez-Mejia, M., 2017, Timing of initial seafloor spreading in
1179 the Newfoundland-Iberia rift: Geology, v. 45, no. 6, p. G38766.1, doi:
1180 10.1130/G38766.1.

1181 Elliott, G.M., and Parson, L.M., 2008, Influence of margin segmentation upon the break-up
1182 of the Hatton Bank rifted margin, NE Atlantic: Tectonophysics, v. 457, no. 3–4, p. 161–
1183 176, doi: 10.1016/j.tecto.2008.06.008.

1184 Enachescu, M.E., 2006, Structural Setting and Petroleum Potential of the Orphan Basin,
1185 offshore Newfoundland and Labrador: Canadian Society of Exploration Geophysicists
1186 Recorder, v. 31, no. 2, p. 5–13.

1187 Engström, J., and Klint, K., 2014, Continental Collision Structures and Post-Orogenic
1188 Geological History of the Kangerlussuaq Area in the Southern Part of the
1189 Nagssugtoqidian Orogen, Central West Greenland: Geosciences, v. 4, p. 316–334, doi:
1190 10.3390/geosciences4040316.

1191 Foulger, G.R., and Anderson, D.L., 2005, A cool model for the Iceland hotspot: Journal of
1192 Volcanology and Geothermal Research, v. 141, no. 1–2, p. 1–22, doi:
1193 10.1016/j.jvolgeores.2004.10.007.

1194 Foulger, G.R., Christiansen, R.L., and Anderson, D.L., 2015, The Yellowstone “hot spot”
1195 track results from migrating basin-range extension: Geological Society of America
1196 Special Paper, v. 514, no. 514, p. SPE514-14, doi: 10.1130/2015.2514(14).

1197 Foulger, G.R., Natland, J.H., and Anderson, D.L., 2005, A source for Icelandic magmas in
1198 remelted Iapetus crust: Journal of Volcanology and Geothermal Research, v. 141, no. 1–
1199 2, p. 23–44, doi: 10.1016/j.jvolgeores.2004.10.006.

1200 Franke, D., 2013, Rifting, lithosphere breakup and volcanism: Comparison of magma-poor
1201 and volcanic rifted margins: Marine and Petroleum Geology, v. 43, no. 0, p. 63–87, doi:
1202 10.1016/j.marpetgeo.2012.11.003.

1203 Frizon De Lamotte, D., Fourdan, B., Leleu, S., Leparmentier, F., and De Clarens, P., 2015,
1204 Style of rifting and the stages of Pangea breakup: Tectonics, v. 34, no. 5, p. 1009–1029,
1205 doi: 10.1002/2014TC003760.

1206 Funck, T., 2003, Crustal structure of the ocean-continent transition at Flemish Cap: Seismic
1207 refraction results: Journal of Geophysical Research, v. 108, no. B11, p. 2531, doi:
1208 10.1029/2003JB002434.

1209 Gaina, C., Gernigon, L., and Ball, P., 2009, Palaeocene-Recent plate boundaries in the NE
1210 Atlantic and the formation of the Jan Mayen microcontinent: Journal of the Geological
1211 Society, v. 166, no. 4, p. 601–616, doi: 10.1144/0016-76492008-112.

1212 Geldmacher, J., Hoernle, K., Bogaard, P. V.D., Duggen, S., and Werner, R., 2005,
1213 New40Ar39Ar age and geochemical data from seamounts in the Canary and Madeira
1214 volcanic provinces: Support for the mantle plume hypothesis: Earth and Planetary
1215 Science Letters, v. 237, no. 1–2, p. 85–101, doi: 10.1016/j.epsl.2005.04.037.

1216 Geng, M., Farquharson, C., Welford, J.K., and Peace, A.L., 2019, 3-D inversion of airborne
1217 gravity gradiometry data for the Budgell Harbour Stock, Newfoundland: A case history
1218 using a probabilistic approach: Geophysics,.

1219 Geoffroy, L., 2005, Volcanic passive margins: Comptes Rendus - Geoscience, v. 337, no. 16,
1220 p. 1395–1408, doi: 10.1016/j.crte.2005.10.006.

1221 Geoffroy, L., Burov, E.B., and Werner, P., 2015, Volcanic passive margins: another way to
1222 break up continents: Scientific Reports, v. 5, p. 14828, doi: 10.1038/srep14828.

1223 Gernigon, L., Blischke, A., Nasuti, A., and Sand, M., 2015, Conjugate volcanic rifted
1224 margins, seafloor spreading, and microcontinent: Insights from new high-resolution
1225 aeromagnetic surveys in the Norway Basin: Tectonics, , no. July, p. 907–933, doi:
1226 10.1002/2014TC003717.

1227 Gernigon, L., Franke, D., Geoffroy, L., Schiffer, C., Foulger, G.R., and Stoker, M., 2019,
1228 Crustal fragmentation, magmatism, and the diachronous opening of the Norwegian-
1229 Greenland Sea: Earth-Science Reviews,.

1230 Gion, A., Williams, S., and Muller, D., 2017, A reconstruction of the Eurekan Orogeny
1231 incorporating deformation constraints: Tectonics, p. 304–320, doi:
1232 10.1002/2015TC004094.

1233 Gouiza, M., Hall, J., and Bertotti, G., 2015, Rifting and pre-rift lithosphere variability in the
1234 Orphan Basin, Newfoundland margin, Eastern Canada: Basin Research, v. 27, no. 4, p.
1235 367–386, doi: 10.1111/bre.12078.

1236 Gouiza, M., Hall, J., and Welford, J.K., 2016, Tectono-stratigraphic evolution and crustal

architecture of the Orphan Basin during North Atlantic rifting: International Journal of Earth Sciences, doi: 10.1007/s00531-016-1341-0.

Gouiza, M., and Paton, D.A., 2019, The role of inherited lithospheric heterogeneities in defining the crustal architecture of rifted margins and the magmatic budget during continental breakup.: Geochemistry, Geophysics, Geosystems,.

Grant, A.C., 1987, Inversion tectonics on the continental margin east of Newfoundland: Geology, v. 15, no. 9, p. 845–848.

Grocott, J., and McCaffrey, K., 2017, Basin Evolution and Destruction in an Early Proterozoic Continental Margin: the Rinkian Fold-Thrust Belt of Central West Greenland: Journal of the Geological Society, doi: 10.1144/jgs2016-109.

Gurnis, M., Turner, M., Zahirovic, S., DiCaprio, L., Spasojevic, S., M??ller, R.D., Boyden, J., Seton, M., Manea, V.C., and Bower, D.J., 2012, Plate tectonic reconstructions with continuously closing plates: Computers and Geosciences, v. 38, no. 1, p. 35–42, doi: 10.1016/j.cageo.2011.04.014.

Gurnis, M., Yang, T., Cannon, J., Turner, M., Williams, S., Flament, N., and Müller, R.D., 2018, Global tectonic reconstructions with continuously deforming and evolving rigid plates: Computers and Geosciences, v. 116, p. 32–41, doi: 10.1016/j.cageo.2018.04.007.

Hansen, J., Jerram, D.A., McCaffrey, K., and Passey, S.R., 2009, The onset of the North Atlantic Igneous Province in a rifting perspective: Geological Magazine, v. 146, no. 03, p. 309, doi: 10.1017/S0016756809006347.

Hardy, R.J.J., Querendez, E., Biancotto, F., Jones, S.M., O'Sullivan, J., and White, N., 2010, New methods of improving seismic data to aid understanding of passive margin evolution: a series of case histories from offshore west of Ireland: Petroleum Geology: From Mature Basins to New Frontiers—Proceedings of the 7th Petroleum Geology Conference, v. 7, p. 1005–1012, doi: 10.1144/0071005.

Hitchen, K., 2004, The geology of the UK Hatton-Rockall margin: Marine and Petroleum Geology, v. 21, no. 8, p. 993–1012, doi: 10.1016/j.marpetgeo.2004.05.004.

Hopper, J.R., Dahl-Jensen, T., Holbrook, W.S., Larsen, H.C., Lizarralde, D., Korenaga, J., Kent, G.M., and Kelemen, P.B., 2003, Structure of the SE Greenland margin from seismic reflection and refraction data: Implications for nascent spreading center subsidence and asymmetric crustal accretion during North Atlantic opening: Journal of Geophysical Research, v. 108, doi: 10.1029/2002jb001996.

Hosseinpour, M., Müller, R.D., Williams, S.E., and Whittaker, J.M., 2013, Full-fit reconstruction of the Labrador Sea and Baffin Bay: Solid Earth, v. 4, no. 2, p. 461–479, doi: 10.5194/se-4-461-2013.

Japsen, P., Bonow, J.M., Peulvast, J.-P., and Wilson, R.W., 2006, Uplift, erosion and fault reactivation in southern West Greenland.: GEUS Field Reports, v. 63.

Jauer, C.D., Oakey, G.N., Williams, G., and Wielens, J.B.W.H., 2014, Saglek Basin in the Labrador Sea, east coast Canada; stratigraphy, structure and petroleum systems: Bulletin of Canadian Petroleum Geology, v. 62, no. 4.

1277 Jones, S.M., White, N., and Lovell, B., 2001, Cenozoic and Cretaceous transient uplift in the
1278 Porcupine Basin and its relationship to a mantle plume: Geological Society, London,
1279 Special Publications, v. 188, no. 1, p. 345–360, doi: 10.1144/GSL.SP.2001.188.01.20.

1280 Joppen, M., and White, R.S., 1990, The structure and subsidence of Rockall Trough from
1281 two-ship seismic experiments: Journal of Geophysical Research, v. 95, no. B12, p.
1282 19821, doi: 10.1029/JB095iB12p19821.

1283 Keen, C.E., Dafoe, L.T., and Dickie, K., 2014, A volcanic province near the Western
1284 termination of the Charlie-Gibbs Fracture Zone at the rifted margin, offshore northeast
1285 Newfoundland: Tectonics, v. 33, no. 6, p. 1133–1153, doi: 10.1002/2014TC003547.

1286 Kerr, A., Ryan, B., Gower, C.F., and Wardle, R.J., 1996, The Makkovik Province: extension
1287 of the Ketilidian Mobile Belt in mainland North America: Geological Society, London,
1288 Special Publications, v. 112, no. 1, p. 155–177, doi: 10.1144/GSL.SP.1996.112.01.09.

1289 Koopmann, H., Brune, S., Franke, D., and Breuer, S., 2014, Linking rift propagation barriers
1290 to excess magmatism at volcanic rifted margins: Geology, v. 42, no. 12, p. 1071–1074,
1291 doi: 10.1130/G36085.1.

1292 Lapointe, P.L., 1979, Paleomagnetism of the Notre Dame Bay lamprophyre dikes,
1293 Newfoundland, and the opening of the North Atlantic Ocean: Canadian Journal of Earth
1294 Sciences, v. 16, no. 9, p. 1823–1831.

1295 Larsen, L.M., Heaman, L.M., Creaser, R.A., Duncan, R.A., Frei, R., and Hutchison, M.,
1296 2009, Tectonomagmatic events during stretching and basin formation in the Labrador
1297 Sea and the Davis Strait: evidence from age and composition of Mesozoic to Palaeogene
1298 dyke swarms in West Greenland: Journal of the Geological Society, v. 166, no. 6, p.
1299 999–1012, doi: 10.1144/0016-76492009-038.

1300 Lau, K.W.H., Louden, K.E., Funck, T., Tucholke, B.E., Holbrook, W.S., Hopper, J.R., and
1301 Christian Larsen, H., 2006, Crustal structure across the Grand Banks–Newfoundland
1302 Basin Continental Margin – II. Results from a seismic reflection profile K.W.:
1303 Geophysical Journal International, v. 167, no. 1, p. 127–156, doi: 10.1111/j.1365-
1304 246X.2006.02988.x.

1305 Lau, K.W.H., Watremez, L., Louden, K.E., and Nedimović, M.R., 2015, Structure of thinned
1306 continental crust across the Orphan Basin from a dense wide-angle seismic profile and
1307 gravity data: Geophysical Journal International, v. 202, no. 3, p. 1969–1992, doi:
1308 10.1093/gji/ggv261.

1309 Leleu, S., Hartley, A.J., van Oosterhout, C., Kennan, L., Ruckwied, K., and Gerdes, K., 2016,
1310 Structural, stratigraphic and sedimentological characterisation of a wide rift system: the
1311 Triassic rift system of the Central Atlantic Domain: Earth-Science Reviews, v. 158, p.
1312 89–124.

1313 Li, Y., and Oldenburg, D., 1998, 3-D inversion of gravity data: Geophysics, v. 63, no. 1, p.
1314 109–119, doi: 10.1190/1.1444302.

1315 Li, Y., and Oldenburg, D., 1996, 3-D inversion of magnetic data: Geophysics, v. 61, no. 2, p.
1316 394–408, doi: 10.1190/1.1443968.

1317 Lister, G.S., Etheridge, M.A., and Symonds, P.A., 1986, Detachment Faulting and the

1318 Evolution of Passive Continental Margins: Geology, v. 14, no. 10, p. 891–892.

1319 Louden, K., Wu, Y., and Tari, G., 2013, Systematic variations in basement morphology and
1320 rifting geometry along the Nova Scotia and Morocco conjugate margins: Geological
1321 Society, London, Special Publications, v. 369, p. 267–287, doi: 10.1144/SP369.9.

1322 Lundin, E., 2002, North Atlantic – Arctic : Overview of sea-floor spreading and rifting
1323 history, *in* Mid Norway plate reconstructions atlas with global and Atlantic perspectives,
1324 p. 41–75.

1325 Lundin, E.R., and Doré, A.G., 2011, Hyperextension, serpentinization, and weakening: A
1326 new paradigm for rifted margin compressional deformation: Geology, v. 39, no. 4, p.
1327 347–350, doi: 10.1130/G31499.1.

1328 Lundin, E.R., Doré, A.G., and Redfield, T.F., 2018, Magmatism and extension rates at rifted
1329 margins: Petroleum Geoscience, p. 32–33.

1330 Magee, C., Jackson, C.A.L., and Schofield, N., 2014, Diachronous sub-volcanic intrusion
1331 along deep-water margins: Insights from the Irish Rockall Basin: Basin Research, v. 26,
1332 no. 1, p. 85–105, doi: 10.1111/bre.12044.

1333 Marillier, F., Hall, J., Hughes, S., Louden, K., Reid, I., Roberts, B., Clowes, R., Coté, T.,
1334 Fowler, J., Guest, S., Lu, H., Luetgert, J., Quinlan, G., Spencer, C., et al., 1994,
1335 LITHOPROBE East onshore-offshore seismic refraction survey -constraints on
1336 interpretation of reflection data in the Newfoundland Appalachians: Tectonophysics, v.
1337 232, no. 1–4, p. 43–58, doi: 10.1016/0040-1951(94)90075-2.

1338 Matthews, K.J., Maloney, K.T., Zahirovic, S., Williams, S.E., Seton, M., and Müller, R.D.,
1339 2016, Global plate boundary evolution and kinematics since the late Paleozoic: Global
1340 and Planetary Change, v. 146, p. 226–250, doi: 10.1016/j.gloplacha.2016.10.002.

1341 McDonnell, A., and Shannon, P.M., 2001, Comparative Tertiary stratigraphic evolution of
1342 the Porcupine and Rockall basins: Geological Society, London, Special Publications , v.
1343 188, no. 1, p. 323–344, doi: 10.1144/GSL.SP.2001.188.01.19.

1344 McKenzie, D., 1978, Some remarks on the development of sedimentary basins: Earth and
1345 Planetary Science Letters, v. 40, no. 1, p. 25–32, doi: 10.1016/0012-821X(78)90071-7.

1346 Müller, R.D., Cannon, J., Qin, X., and Watson, R.J., 2018, GPlates – Building a Virtual Earth
1347 Through Deep Time: Geochemistry Geophysics Geosystems, doi:
1348 10.1029/2018GC007584.

1349 Müller, R.D., Seton, M., Zahirovic, S., Williams, S.E., Matthews, K.J., Wright, N.M.,
1350 Shephard, G.E., Maloney, K.T., Barnett-Moore, N., Hosseinpour, M., Bower, D.J., and
1351 Cannon, J., 2016, Ocean Basin Evolution and Global-Scale Plate Reorganization Events
1352 Since Pangea Breakup: Annual Review of Earth and Planetary Sciences, v. 44, no. 1, p.
1353 107–138, doi: 10.1146/annurev-earth-060115-012211.

1354 Müller, R.D., Zahirovic, S., Williams, S.E., Cannon, J., Seton, M., Bower, D.J., Tetley, M.,
1355 Heine, C., Le Breton, E., Liu, S., Russell, S.H.J., Yang, T., Leonard, J., and Gurnis, M.,
1356 2019, A global plate model including lithospheric deformation along major rifts and
1357 orogens since the Triassic: Tectonics, doi: 10.1029/2018TC005462.

1358 Naylor, D., and Shannon, P.M., 2005, The structural framework of the Irish Atlantic Margin,
1359 *in* Petroleum Geology: North-West Europe and Global Perspectives—Proceedings of the
1360 6th Petroleum Geology Conference, p. 1009–1021.

1361 Nielsen, T.K., 2002, Formation of volcanic rifted margins: Are temperature anomalies
1362 required? Geophysical Research Letters, v. 29, no. 21, p. 2022, doi:
1363 10.1029/2002GL015681.

1364 Nirrengarten, M., Manatschal, G., Tugend, J., Kusznir, N., and Sauter, D., 2018, Kinematic
1365 evolution of the southern North Atlantic: implications for the formation of hyper-
1366 extended rift systems: Tectonics, p. 2, doi: 10.1002/2017TC004495.

1367 O'Reilly, B.M., Hauser, F., Ravaut, C., Shannon, P.M., and Readman, P.W., 2006, Crustal
1368 thinning, mantle exhumation and serpentinization in the Porcupine Basin, offshore
1369 Ireland: evidence from wide-angle seismic data: Journal of the Geological Society, v.
1370 163, no. 5, p. 775–787, doi: 10.1144/0016-76492005-079.

1371 Oakey, G.N., and Chalmers, J. a, 2012, A new model for the Paleogene motion of Greenland
1372 relative to North America : Plate reconstructions of the Davis Strait and Nares Strait
1373 regions between Canada and Greenland: Journal of Geophysical Research: Solid Earth,
1374 v. 117, no. B10, p. 1–28, doi: 10.1029/2011JB008942.

1375 Pe-Piper, G., Jansa, L.F., and Lambert, R.S.J., 1992, Early Mesozoic magmatism on the
1376 eastern Canadian margin: Petrogenetic and tectonic significance: Geological Society of
1377 America Special Paper, v. 268, no. 2.

1378 Pe-Piper, G., Meredyk, S., Zhang, Y., Piper, D.J.W., and Edinger, E., 2013, Petrology and
1379 tectonic significance of seamounts within transitional crust east of Orphan Knoll,
1380 offshore eastern Canada: Geo-Marine Letters, v. 33, no. 6, p. 433–447, doi:
1381 10.1007/s00367-013-0342-2.

1382 Pe-Piper, G., Piper, D.J.W., Jansa, L.F., and de Jonge, A., 2007, Early Cretaceous opening of
1383 the North Atlantic Ocean: Implications of the petrology and tectonic setting of the Fogo
1384 seamounts off the SW Grand Banks, Newfoundland: Bulletin of the Geological Society
1385 of America, v. 119, no. 5–6, p. 712–724, doi: 10.1130/B26008.1.

1386 Peace, A.L., Dempsey, E.D., Schiffer, C., Welford, J.K., and Ken, J.W., 2018a, Evidence for
1387 basement reactivation during the opening of the Labrador Sea from the Makkovik
1388 Province, Labrador, Canada: Insights from field-data and numerical models:
1389 Geosciences,.

1390 Peace, A.L.L., Dempsey, E.D.D., Schiffer, C., Welford, J.K., Ken, J.W., McCaffrey, K.,
1391 Imber, J., and Phethean, J., 2018b, Evidence for Basement Reactivation during the
1392 Opening of the Labrador Sea from the Makkovik Province, Labrador, Canada: Insights
1393 from Field Data and Numerical Models: Geosciences, v. 8, no. 8, p. 308, doi:
1394 10.3390/geosciences8080308.

1395 Peace, A.L., Foulger, G.R., Schiffer, C., and Mccaffrey, K.J.W., 2017a, Evolution of
1396 Labrador Sea–Baffin Bay: Plate or Plume Processes? Geoscience Canada, v. 44, no. 3,
1397 doi: 10.12789/geocanj.2017.44.120.

1398 Peace, A.L., McCaffrey, K.J.W., Imber, J., Hobbs, R., van Hunen, J., and Gerdes, K., 2017b,
1399 Quantifying the influence of sill intrusion on the thermal evolution of organic-rich

1400 sedimentary rocks in nonvolcanic passive margins: An example from ODP 210-1276,
1401 offshore Newfoundland, Canada: Basin Research, v. 29, no. 3, p. 249–265, doi:
1402 10.1111/bre.12131.

1403 Peace, A., McCaffrey, K.J.W., Imber, J., van Hunen, J., Hobbs, R., and Wilson, R., 2018c,
1404 The role of pre-existing structures during rifting, continental breakup and transform
1405 system development, offshore West Greenland: Basin Research, v. 30, no. 3, p. 373–
1406 394, doi: 10.1111/bre.12257.

1407 Peace, A., McCaffrey, K.J.W., Imber, J., Phethean, J., Nowell, G., Gerdes, K., and Dempsey,
1408 E., 2016, An evaluation of Mesozoic rift-related magmatism on the margins of the
1409 Labrador Sea: Implications for rifting and passive margin asymmetry: Geosphere, v. 12,
1410 no. 6, doi: 10.1130/GES01341.1.

1411 Peace, A.L., Welford, J.K., Geng, M., Sandeman, H., Gaetz, B.D., and Ryan, S.S., 2018d,
1412 Rift-related magmatism on magma-poor margins: Structural and potential-field analyses
1413 of the Mesozoic Notre Dame Bay intrusions, Newfoundland, Canada and their link to
1414 North Atlantic Opening: Tectonophysics, v. 745, no. October, p. 24–45, doi:
1415 10.1016/j.tecto.2018.07.025.

1416 Peron-Pinvidic, G., Gernigon, L., Gaina, C., and Ball, P., 2012a, Insights from the Jan Mayen
1417 system in the Norwegian-Greenland sea-I. Mapping of a microcontinent: Geophysical
1418 Journal International, v. 191, no. 2, p. 385–412, doi: 10.1111/j.1365-
1419 246X.2012.05639.x.

1420 Peron-Pinvidic, G., Gernigon, L., Gaina, C., and Ball, P., 2012b, Insights from the Jan Mayen
1421 system in the Norwegian-Greenland Sea-II. Architecture of a microcontinent:
1422 Geophysical Journal International, v. 191, no. 2, p. 413–435, doi: 10.1111/j.1365-
1423 246X.2012.05623.x.

1424 Peron-Pinvidic, G., and Manatschal, G., 2010, From microcontinents to extensional
1425 allochthons: witnesses of how continents rift and break apart? Petroleum Geoscience, v.
1426 16, no. 3, p. 189–197, doi: 10.1144/1354-079309-903.

1427 Peron-Pinvidic, G., Manatschal, G., Minshull, T.A., and Sawyer, D.S., 2007,
1428 Tectonosedimentary evolution of the deep Iberia-Newfoundland margins: Evidence for a
1429 complex breakup history: Tectonics, v. 26, no. 2, p. TC2011, doi:
1430 10.1029/2006TC001970.

1431 Petersen, K.D., Schiffer, C., and Nagel, T.J., 2018, LIP formation and protracted lower
1432 mantle upwelling induced by rifting and delamination: Scientific Reports, p. 1–11, doi:
1433 10.1038/s41598-018-34194-0.

1434 Phethean, J., Kalnins, L., van Hunen, J., Biffi, P.G., Davies, R.J., and McCaffrey, K.J.W.,
1435 2016, Madagascar's escape from Africa: A high-resolution plate reconstruction for the
1436 Western Somali Basin and implications for supercontinent dispersal: Geochemistry,
1437 Geophysics, Geosystems, v. 17, no. 7, p. 2825–2834, doi: 10.1002/2016GC006406.

1438 Picazo, S., Müntener, O., Manatschal, G., Bauville, A., Karner, G., and Johnson, C., 2016,
1439 Mapping the nature of mantle domains in Western and Central Europe based on
1440 clinopyroxene and spinel chemistry: Evidence for mantle modification during an
1441 extensional cycle: Lithos, v. 266–267, no. September 2016, p. 233–263, doi:
1442 10.1016/j.lithos.2016.08.029.

1443 Polteau, S., Mazzini, A., Hansen, G., Planke, S., Jerram, D.A., Millett, J., and Abdelmalak,
1444 M.M., 2018, The pre-breakup stratigraphy and petroleum system of the Southern Jan
1445 Mayen Ridge revealed by seafloor sampling: Tectonophysics, doi:
1446 10.1016/j.tecto.2018.04.016.

1447 Prada, M., Lavoué, F., Saqab, M.M., Reilly, B.M.O., Lebedev, S., Walsh, J.J., and Childs, C.,
1448 2018, Across - axis variations in petrophysical properties of the North Porcupine Basin ,
1449 offshore Ireland: New insights from long - streamer traveltime tomography: , no. June,
1450 p. 1–18, doi: 10.1111/bre.12308.

1451 Rattey, R.P., and Hayward, A.B., 1993, Sequence stratigraphy of a failed rift system: the
1452 Middle Jurassic to Early Cretaceous basin evolution of the Central and Northern North
1453 Sea: Petroleum Geology of Northwest Europe: Proceedings of the 4th Conference on
1454 Petroleum Geology of NW. Europe, at the Barbican Centre, London, v. 1, p. 215–249,
1455 doi: 10.1144/0040215.

1456 Reston, T.J., 2009, The structure, evolution and symmetry of the magma-poor rifted margins
1457 of the North and Central Atlantic: A synthesis: Tectonophysics, v. 468, no. 1–4, p. 6–27,
1458 doi: 10.1016/j.tecto.2008.09.002.

1459 Reston, T.J., Gaw, V., Pennell, J., Klaeschen, D., Stubenrauch, A., and Walker, I., 2004,
1460 Extreme crustal thinning in the south Porcupine Basin and the nature of the Porcupine
1461 Median High: implications for the formation of non-volcanic rifted margins: Journal of
1462 the Geological Society, v. 161, no. 5, p. 783–798, doi: 10.1144/0016-764903-036.

1463 Reston, T.J., Pennell, J., Stubenrauch, A., Walker, I., and Perez-Gussinye, M., 2001,
1464 Detachment faulting, mantle serpentinization, and serpentinite-mud, volcanism beneath
1465 the Porcupine Basin, southwest of Ireland: Geology, v. 29, no. 7, p. 587–590, doi:
1466 10.1130/0091-7613(2001)029<0587:DFMSAS>2.0.CO;2.

1467 Roberts, A.M., Alvey, A.D., and Kusznir, N.J., 2018, Crustal structure and heat-flow history
1468 in the UK Rockall Basin, derived from backstripping and gravity-inversion analysis:
1469 Petroleum Geoscience,.

1470 Rowley, D.B., and Lottes, A.L., 1988, Plate-kinematic reconstructions of the North Atlantic
1471 and Arctic: Late Jurassic to present: Tectonophysics, v. 155, no. 1–4, p. 73–120.

1472 Schiffer, C., Peace, A., Phethean, J., Gernigon, L., McCaffrey, K.J.W., Petersen, K.D., and
1473 Foulger, G.R., 2018, The Jan Mayen Microplate Complex and the Wilson Cycle: in
1474 Tectonic Evolution: 50 Years of the Wilson Cycle Concept: Geological Society of
1475 London, Special Publications, v. 470, doi: 10.1144/SP470.2.

1476 Schofield, N., Jolley, D., Holford, S., Archer, S., Watson, D., Hartley, A., Howell, J.,
1477 Muirhead, D., Underhill, J., and Green, P., 2018, Challenges of future exploration within
1478 the UK Rockall Basin: Petroleum geology of Northwest Europe: 50 years of learning.
1479 Proceedings of the 8th Petroleum Geology Conference, p. 1–19, doi: 10.1144/PGC8.37.

1480 Scotchman, I.C., Doré, A.G., and Spencer, A.M., 2018, Petroleum systems and results of
1481 exploration on the Atlantic margins of the UK, Faroes and Ireland: what have we learnt?
1482 Petroleum geology of Northwest Europe: 50 years of learning. Proceedings of the 8th
1483 Petroleum Geology Conference, p. 11pp, doi: 10.1144/PGC8.14.

1484 Seton, M., Müller, R.D., Zahirovic, S., Gaina, C., Torsvik, T., Shephard, G., Talsma, A.,

1485 Gurnis, M., Turner, M., Maus, S., and Chandler, M., 2012, Global continental and ocean
1486 basin reconstructions since 200Ma: Earth-Science Reviews, v. 113, no. 3–4, p. 212–270,
1487 doi: 10.1016/j.earscirev.2012.03.002.

1488 Shannon, P., 2018, Old challenges, new developments and new plays in Irish offshore
1489 exploration: Petroleum Geology of Northwest Europe: 50 Years of Learning -
1490 Proceedings of the 8th Petroleum Geology Conference, p. 171–185, doi:
1491 10.1144/PGC8.12.

1492 Shannon, P.M., 1991, The development of Irish offshore sedimentary basins: Journal of the
1493 Geological Society, v. 148, no. 1, p. 181–189, doi: 10.1144/gsjgs.148.1.0181.

1494 Shannon, P.M., Jacob, A.W.B., O'Reilly, B.M., Hauser, F., Readman, P.W., and Makris, J.,
1495 1999, Structural setting, geological development and basin modelling in the Rockall
1496 Trough: Petroleum Geology of Northwest Europe: Proceedings of the 5th Conference on
1497 the Petroleum Geology of Northwest Europe, p. 421–431, doi: 10.1144/0050421.

1498 Shorttle, O., Maclennan, J., and Lambart, S., 2014, Quantifying lithological variability in the
1499 mantle: Earth and Planetary Science Letters, v. 395, p. 24–40, doi:
1500 10.1016/j.epsl.2014.03.040.

1501 Sibuet, J.-C., Srivastava, S.P., Enachescu, M., and Karner, G.D., 2007, Early Cretaceous
1502 motion of Flemish Cap with respect to North America: implications on the formation of
1503 Orphan Basin and SE Flemish Cap Galicia Bank conjugate margins: Geological Society,
1504 London, Special Publications, v. 282, no. 1, p. 63–76, doi: 10.1144/SP282.4.

1505 Sinclair, I.K., 1995, Sequence stratigraphic response to Aptian-Albian rifting in conjugate
1506 margin basins: a comparison of the Jeanne d'Arc Basin, offshore Newfoundland, and the
1507 Porcupine Basin, offshore Ireland: Geological Society, London, Special Publications, v.
1508 90, no. 1, p. 29–49.

1509 Sinclair, I.K., Shannon, P.M., Williams, B.P.J., Harker, S.D., and Mooren, J.G., 1994,
1510 Tectonic control on sedimentary evolution of three North Atlantic borderland Mesozoic
1511 basins1: Basin Research, v. 6, no. 4, p. 193–217, doi: 10.1111/j.1365-
1512 2117.1994.tb00085.x.

1513 Skogseid, J., 2010, The Orphan Basin – a key to understanding the kinematic linkage
1514 between North and NE Atlantic Mesozoic rifting: II Central and North Atlantic
1515 Conjugate Margins Conference, v. II, p. 13–23.

1516 Smith, W.H., and Sandwell, D., 1997, Global Sea Floor Topography from Satellite Altimetry
1517 and Ship Depth Soundings: Science, v. 277, no. 5334, p. 1956–1962, doi:
1518 10.1126/science.277.5334.1956.

1519 Srivastava, S.P., 1978, Evolution of the Labrador Sea and its bearing on the early evolution
1520 of the North Atlantic: Geophysical Journal International, v. 52, no. 2, p. 313–357, doi:
1521 10.1111/j.1365-246X.1978.tb04235.x.

1522 Srivastava, S.P., and Roest, W.R., 1999, Extent of oceanic crust in the Labrador Sea: Marine
1523 and Petroleum Geology, v. 16, no. 1, p. 65–84, doi: 10.1016/S0264-8172(98)00041-5.

1524 St-Onge, M.R., Van Gool, J.A.M., Garde, A.A., Scott, D.J., Gool, J.A.M. Van, Garde, A.A.,
1525 Scott, D.J., Van Gool, J.A.M., Garde, A.A., and Scott, D.J., 2009, Correlation of

1526 Archaean and Palaeoproterozoic units between northeastern Canada and western
1527 Greenland: constraining the pre-collisional upper plate accretionary history of the Trans-
1528 Hudson orogen: Geological Society, London, Special Publications, v. 318, no. 1, p. 193–
1529 235, doi: 10.1144/sp318.7.

1530 Stoker, M.S., Stewart, M.A., Shannon, P.M., Bjerager, M., and Nielsen, T., 2016, An
1531 overview of the Upper Palaeozoic – Mesozoic stratigraphy of the NE Atlantic region:
1532 The NE Atlantic Region: A Reappraisal of Crustal Structure, Tectonostratigraphy and
1533 Magmatic Evolution, v. 447, p. 11–68, doi: 10.1144/SP447.2.

1534 Štolfová, K., and Shannon, P.M., 2009, Permo-Triassic development from Ireland to Norway:
1535 basin architecture and regional controls: Geological Journal, v. 44, no. 6, p. 652–676.

1536 Strong, D.F., and Harris, A., 1974, The Petrology of Mesozoic Alkaline Intrusives of Central
1537 Newfoundland: Canadian Journal of Earth Sciences, v. 11, p. 1208–1219, doi:
1538 10.1139/e74-114.

1539 Suckro, S.K.S.K., Gohl, K., Funck, T., Heyde, I., Schreckenberger, B., Gerlings, J., and
1540 Damm, V., 2013, The Davis Strait crust-a transform margin between two oceanic
1541 basins: Geophysical Journal International, v. 193, no. 1, p. 78–97, doi:
1542 10.1093/gji/ggs126.

1543 Tankard, A.J., and Welsink, H.J., 1987, Extensional tectonics and stratigraphy of Hibernia oil
1544 field, Grand Banks, Newfoundland: AAPG Bulletin, v. 71, no. 10, p. 1210–1232.

1545 Tate, M.P., 1993, Structural framework and tectono-stratigraphic evolution of the Porcupine
1546 Seabight Basin, offshore Western Ireland: Marine and Petroleum Geology, v. 10, no. 2,
1547 p. 95–123, doi: 10.1016/0264-8172(93)90016-L.

1548 Tate, M.P., and Dobson, M.R., 1988, Syn- and post-rift igneous activity in the Porcupine
1549 Seabight Basin and adjacent continental margin W of Ireland: Geological Society,
1550 London, Special Publications, v. 39, no. 1, p. 309 LP-334.

1551 Tate, M.P., Dodd, C.D., and Grant, N.T., 1999, The northeast Rockall basin and its
1552 significance in the evolution of the Rockall-Faeroes/East Greenland rift system:
1553 Petroleum Geology of Northwest Europe: Proceedings of the 5th Conference on the
1554 Petroleum Geology of Northwest Europe, v. 1, no. c, p. 391–406, doi: 10.1144/0050391.

1555 Tavani, S., Bertok, C., Granado, P., Piana, F., Salas, R., Vigna, B., and Muṇoz, J.A., 2018,
1556 The Iberia-Eurasia plate boundary east of the Pyrenees: Earth-Science Reviews,.

1557 Thomson, K., 2005, Extrusive and intrusive magmatism in the North Rockall Trough:
1558 Petroleum Geology Conference series, v. 6, p. 1621–1630, doi: 10.1144/0061621.

1559 Tucholke, B.E., Sawyer, D.S., and Sibuet, J.-C., 2007, Breakup of the Newfoundland Iberia
1560 rift: Geological Society, London, Special Publications, v. 282, no. 1, p. 9–46, doi:
1561 10.1144/SP282.2.

1562 Tucholke, B.E., and Sibuet, J., 2007, Leg 210 synthesis: tectonic, magmatic, and sedimentary
1563 evolution of the Newfoundland-Iberia rift: Proceedings of the Ocean Drilling Program,
1564 Scientific Results Volume 210, v. 210, p. 1–56, doi: 10.2973/odp.proc.sr.210.101.2007.

1565 Umpleby, D.C., 1979, Geology of the Labrador Shelf: Geological Survey of Canada, v. 79–

13.

Vissers, R.L.M., and Meijer, P.T., 2012a, Iberian plate kinematics and Alpine collision in the Pyrenees: Earth-Science Reviews, v. 114, no. 1–2, p. 61–83, doi: 10.1016/j.earscirev.2012.05.001.

Vissers, R.L.M., and Meijer, P.T., 2012b, Mesozoic rotation of Iberia: Subduction in the Pyrenees? Earth-Science Reviews, v. 110, no. 1–4, p. 93–110, doi: 10.1016/j.earscirev.2011.11.001.

Watremez, L., Helen Lau, K.W., Nedimović, M.R., and Louden, K.E., 2015, Traveltime tomography of a dense wide-angle profile across Orphan Basin: Geophysics, v. 80, no. 3, p. B69–B82, doi: 10.1190/geo2014-0377.1.

Watremez, L., Prada, M., Minshull, T., O'Reilly, B., Chen, C., Reston, T., Shannon, P., Wagner, G., Gaw, V., Klaeschen, D., Edwards, R., and Lebedev, S., 2018, Deep structure of the Porcupine Basin from wide-angle seismic data: Geological Society, London, Petroleum Geology Conference series, v. 8, p. PGC8.26, doi: 10.1144/PGC8.26.

Welford, J.K., Hall, J., Sibuet, J.C., and Srivastava, S.P., 2010, Structure across the northeastern margin of Flemish Cap, offshore Newfoundland from Erable multichannel seismic reflection profiles: Evidence for a transtensional rifting environment: Geophysical Journal International, v. 183, no. 2, p. 572–586, doi: 10.1111/j.1365-246X.2010.04779.x.

Welford, J.K., Peace, A.L., Geng, M., Dehler, S.A., and Dickie, K., 2018, Crustal structure of Baffin Bay from constrained three-dimensional gravity inversion and deformable plate tectonic models: Geophysical Journal International, doi: 10.1093/gji/ggy193.

Welford, J.K., Shannon, P.M., O'Reilly, B.M., Hall, J., Reilly, B.M.O., and Hall, J., 2012, Comparison of lithosphere structure across the Orphan Basin – Flemish Cap and Irish Atlantic conjugate continental margins from constrained 3D gravity inversions: Journal of the Geological Society, v. 169, no. 4, p. 405–420, doi: 10.1144/0016-76492011-114.Comparison.

White, R.S., 1992, Magmatism during and after continental break-up: Geological Society, London, Special Publications, v. 68, no. 1, p. 1–16, doi: 10.1144/GSL.SP.1992.068.01.01.

White, R., and McKenzie, D., 1989, Magmatism at rift zones: The generation of volcanic continental margins and flood basalts: Journal of Geophysical Research, v. 94, no. B6, p. 7685, doi: 10.1029/JB094iB06p07685.

White, N., Tate, M., and Conroy, J.-J., 1992, Lithospheric stretching in the Porcupine Basin, west of Ireland: Geological Society, London, Special Publications, v. 62, no. 1, p. 327 LP-331.

Whittaker, R.C., 2016, A New Deformable Plate Reconstruction of the Irish – Newfoundland Conjugate Margin: , no. June 2012, p. 1–4.

Wilkinson, C.M., Ganerød, M., Hendriks, B.W.H., and Eide, E.A., 2016, Compilation and appraisal of geochronological data from the North Atlantic Igneous Province (NAIP):

Geological Society Special Publications,.

Williams, S., Flament, N., Heine, C., Vazifehshenas, M.H., Seton, M., and Gurnis, M., 2012a, Geodynamic modeling of passive margin systems from tectonic reconstructions with deforming plate boundaries: Geophys. Res. Abstracts, v. 14, p. 6830.

Williams, S.E., Müller, R.D., Landgrebe, T.C.W., and Whittaker, J.M., 2012b, An open-source software environment for visualizing and refining plate tectonic reconstructions using high-resolution geological and geophysical data sets: GSA Today, v. 22, no. 4–5, p. 4–9, doi: 10.1130/GSATG139A.1.THE.

Wilson, R.W., Klint, K.E.S., Van Gool, J.A.M., McCaffrey, K.J.W., Holdsworth, R.E., and Chalmers, J.A., 2006, Faults and fractures in central West Greenland: onshore expression of continental break-up and sea-floor spreading in the Labrador–Baffin Bay Sea: Geological Survey Of Denmark And Greenland Bulletin, v. 11, p. 185–204.

Yang, Y.T., 2012, Tectonostratigraphic evolution of the northern Porcupine Basin, Irish Atlantic margin, during the Late Jurassic-Early Cretaceous, implication for a regional compressional event: Marine and Petroleum Geology, v. 36, no. 1, p. 140–153, doi: 10.1016/j.marpetgeo.2012.05.003.

Figures

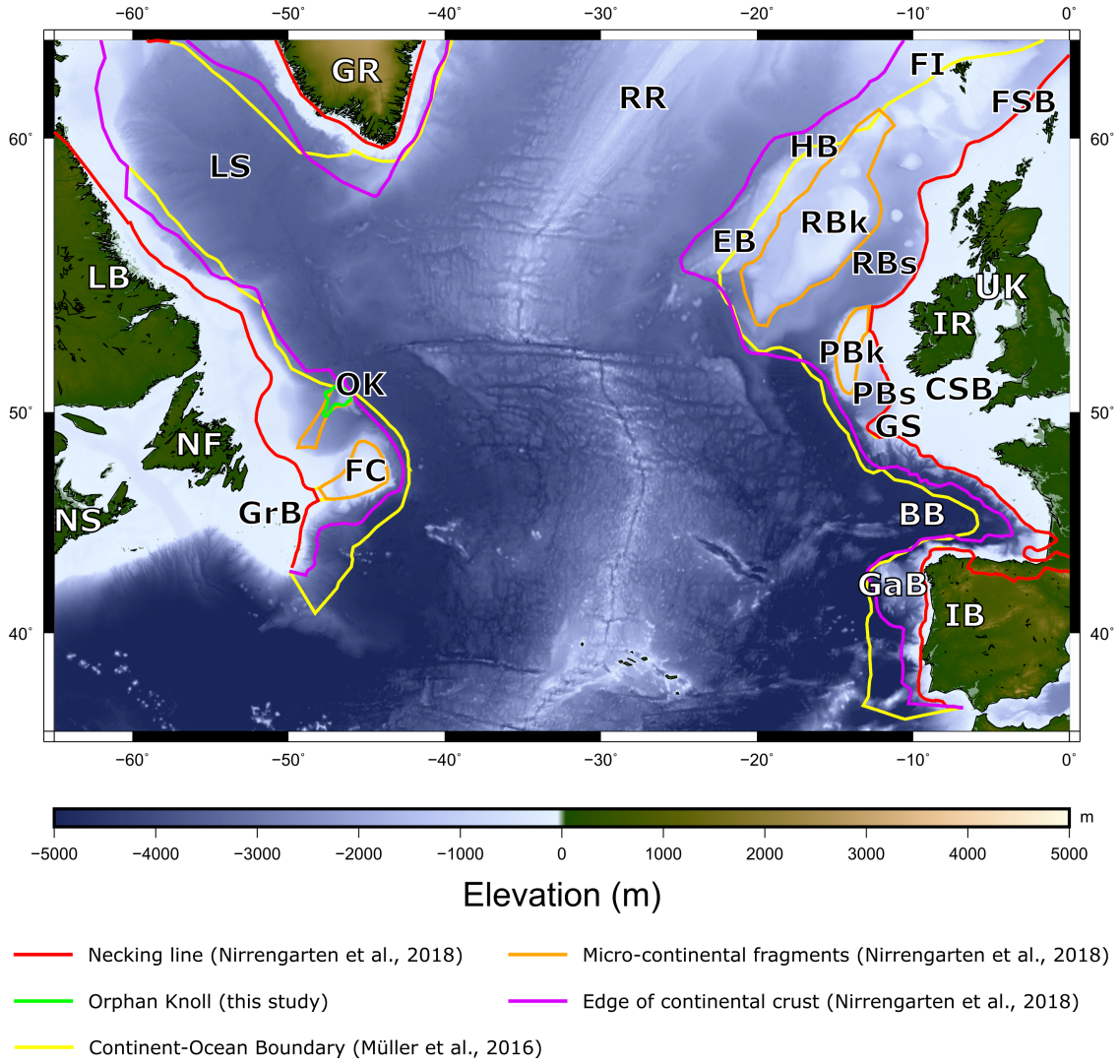

Figure 1

Overview of the southern North Atlantic study area and the main inputs for the GPlates models. The Müller et al. (2016) COB has been cropped to just the segments used in the deformable models. Elevation data from Smith and Sandwell V18.1 (Smith and Sandwell, 1997). AGFZ = Azores-Gibraltar Fracture Zone, BB = Bay of Biscay, CGFZ = Charlie-Gibbs Fracture Zone, CSB = Celtic Sea Basin, EB = Edoras Bank, FC = Flemish Cap, FI = Faroe Islands, FSB = Faroe-Shetland Basin, GaB = Galicia Bank, GrB = Grand Banks, GR = Greenland, GS = Goban Spur, HB = Hatton Bank, IB = Iberia, IR = Ireland, LB = Labrador, LS = Labrador Sea, MAR = Mid-Atlantic Ridge, NF = Newfoundland, NS = Nova Scotia, OB = Orphan Basin, OK = Orphan Knoll, PBk = Porcupine Bank, PBs = Porcupine Basin, QB = Quebec, RBk = Rockall Bank, RBs = Rockall Basin, RR = Reykjanes Ridge, UK = United Kingdom

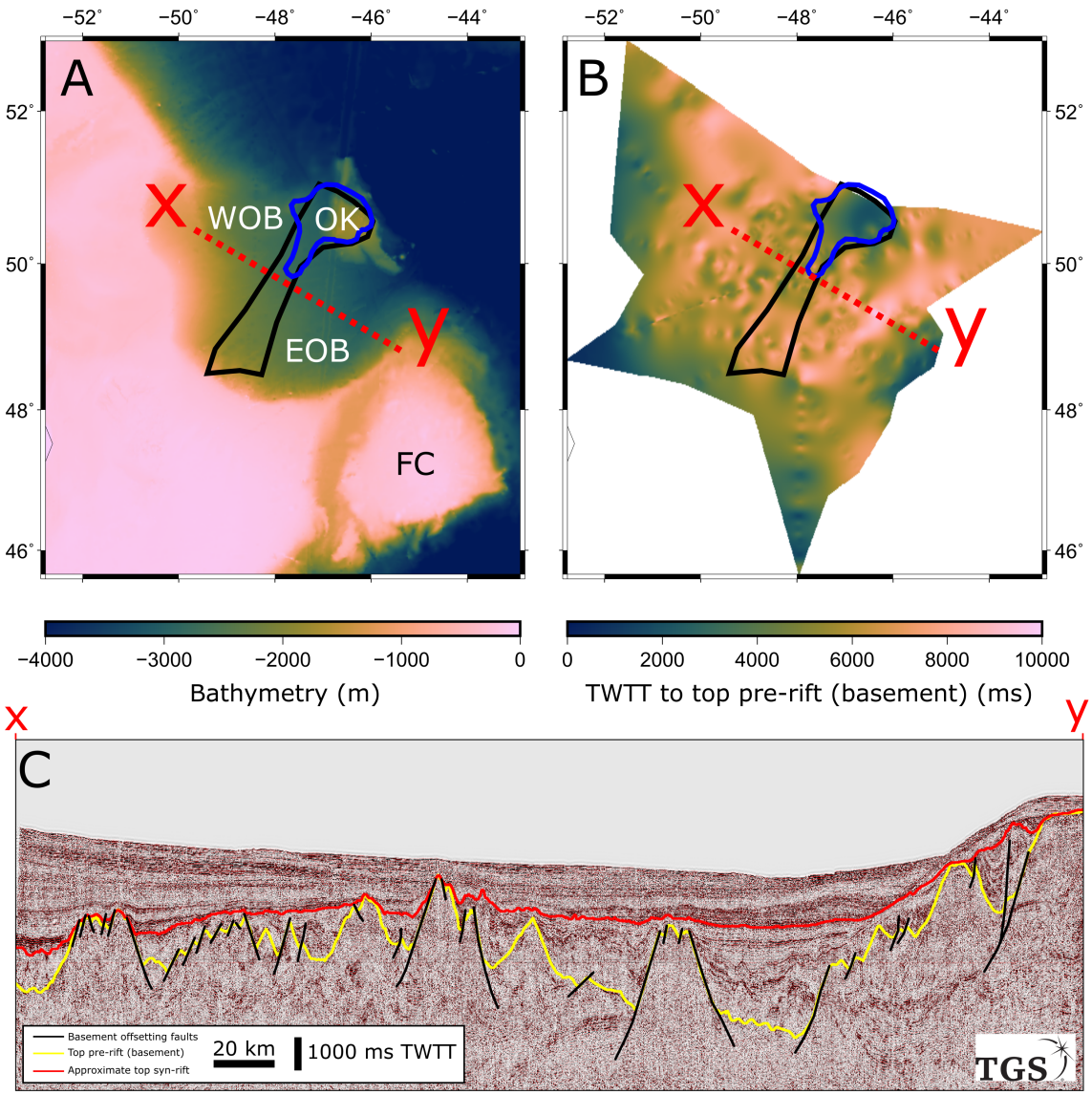

Figure 2

A) Bathymetry of the Orphan Basin (Smith and Sandwell V18.1) overlain by the geometry of the Orphan Knoll block from Nirrengarten et al. (2018) (black polygon) and the geometry derived during this study (blue polygon). The geometry shown by the black polygon is used in Model 2, whilst the geometry shown in blue is used in Models 3 and 6a-d. B) Depth (in two-way-travel time, TWTT) to the seismic basement horizon in the Orphan Basin as used to define a smaller geometry for the Orphan Knoll. C) Representative seismic reflection profile from the 2001 TGS survey through both the East and West Orphan sub-basins with the top pre-rift basement horizon shown in yellow (as used to produce the surface in B) and the approximate top syn-rift horizon in red. We would like to acknowledge TGS for the provision of this data shown in this figure. EOB = East Orphan Basin, FC = Flemish Cap, OK = Orphan Knoll and, WOB = West Orphan Basin.

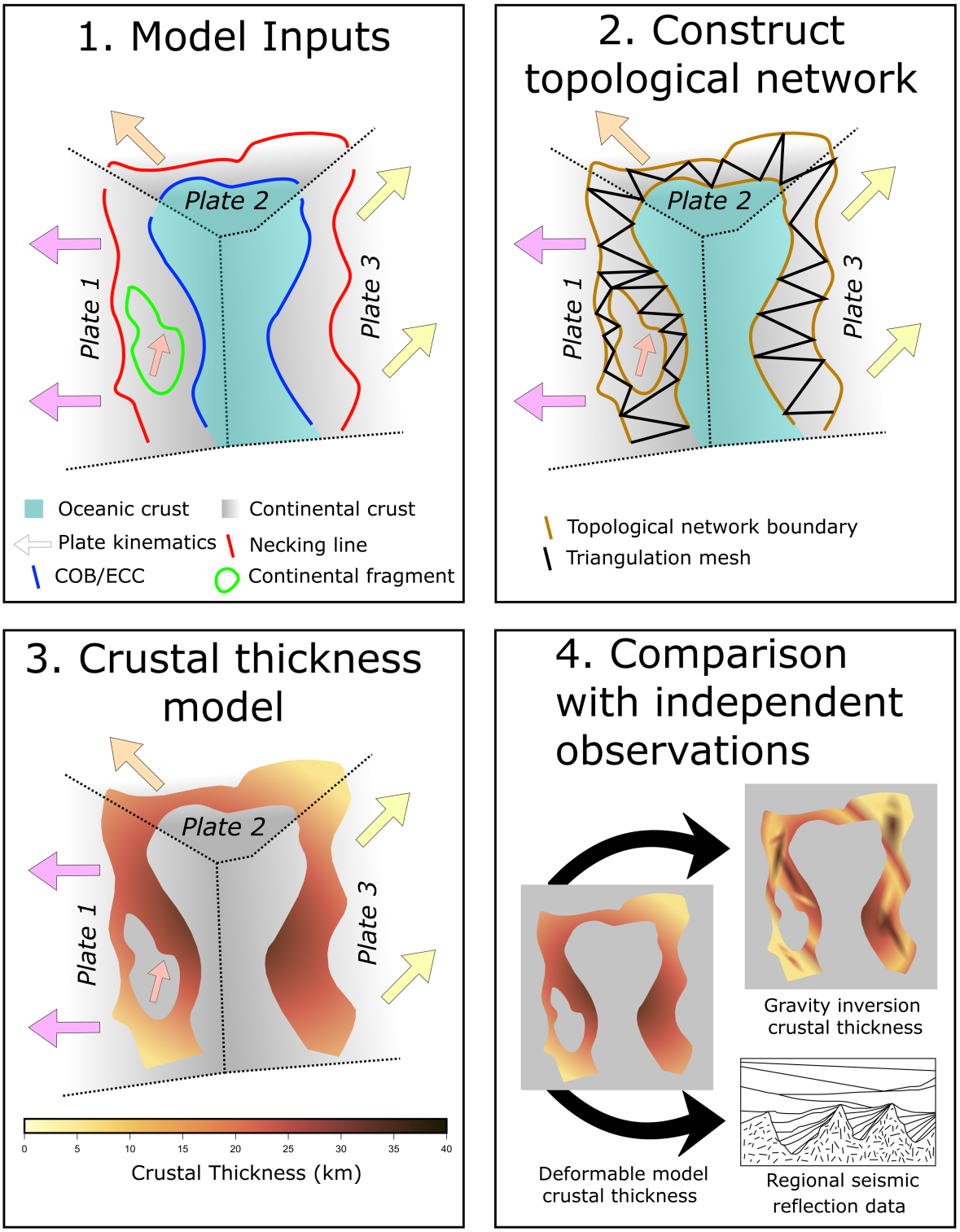

Figure 3

Schematic depiction of the GPlates deformable modelling workflow utilised herein following the method described in Gurnis et al. (2018). COB = Continent-Ocean boundary, and ECC = edge of continental crust.

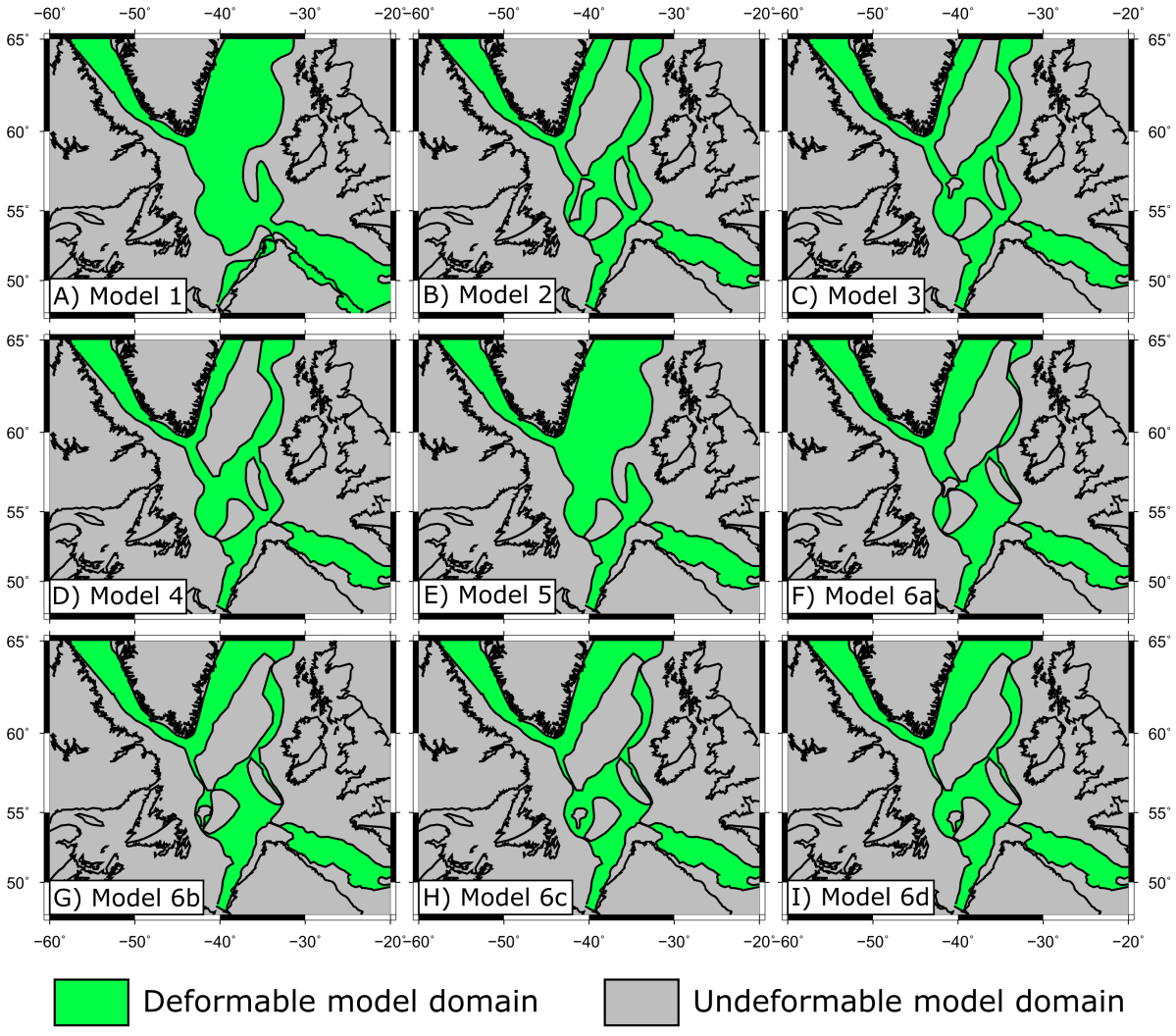

Figure 4

Initial model setup showing the deformable mesh domain in green with uniform, 30 km thick, homogeneous crust at 200 Ma for: A) Model 1, B) Model 2, C) Model 3, D) Model 4, E) Model 5, F) Model 6a, G) Model 6b, H) Model 6c and I) Model 6d. The most northern extent of the modelled domains is slightly greater than shown on this figure but is not included here at it is beyond the primary region of interest.

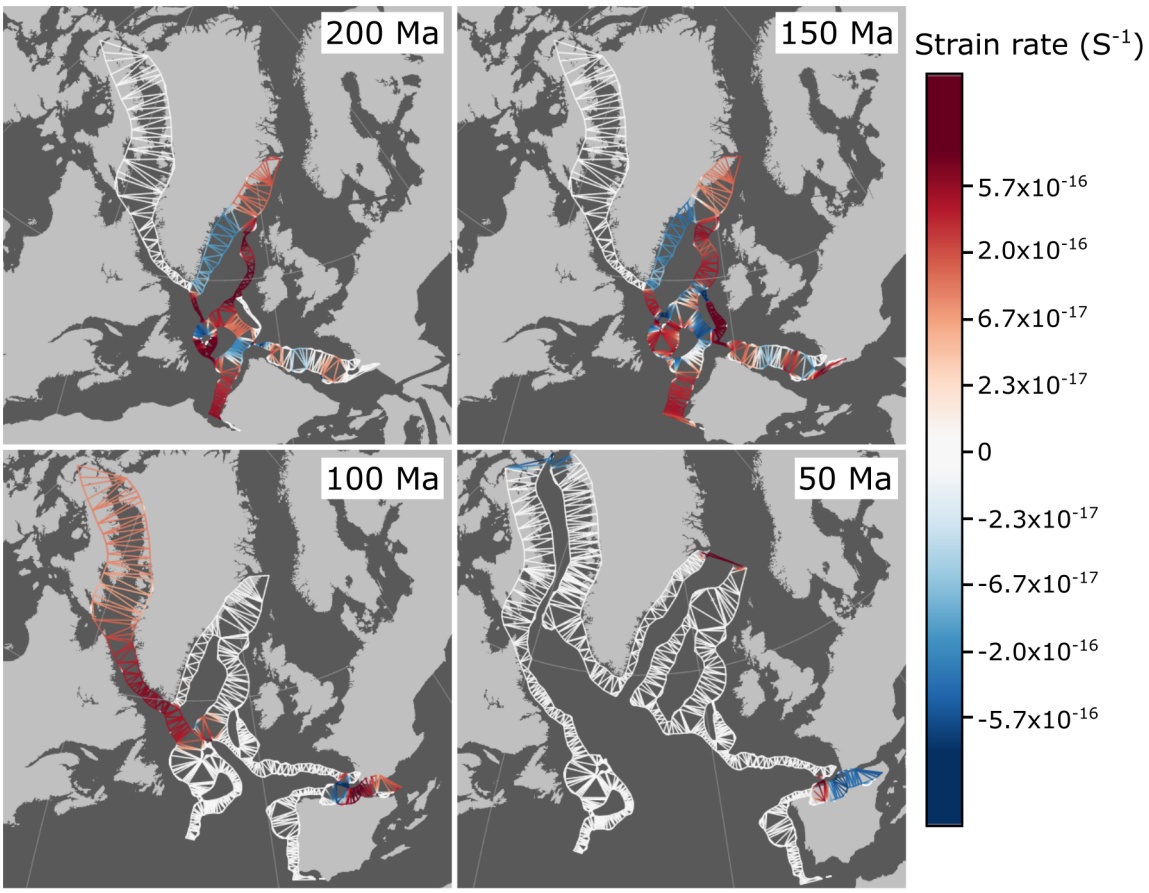

Figure 5 – Evolution of the strain mesh in GPlates used in model 6c, shown with a fixed Greenland plate at 200 Ma, 150 Ma, 100 Ma and 50 Ma. The strain mesh in the other models is of comparable density and distribution.

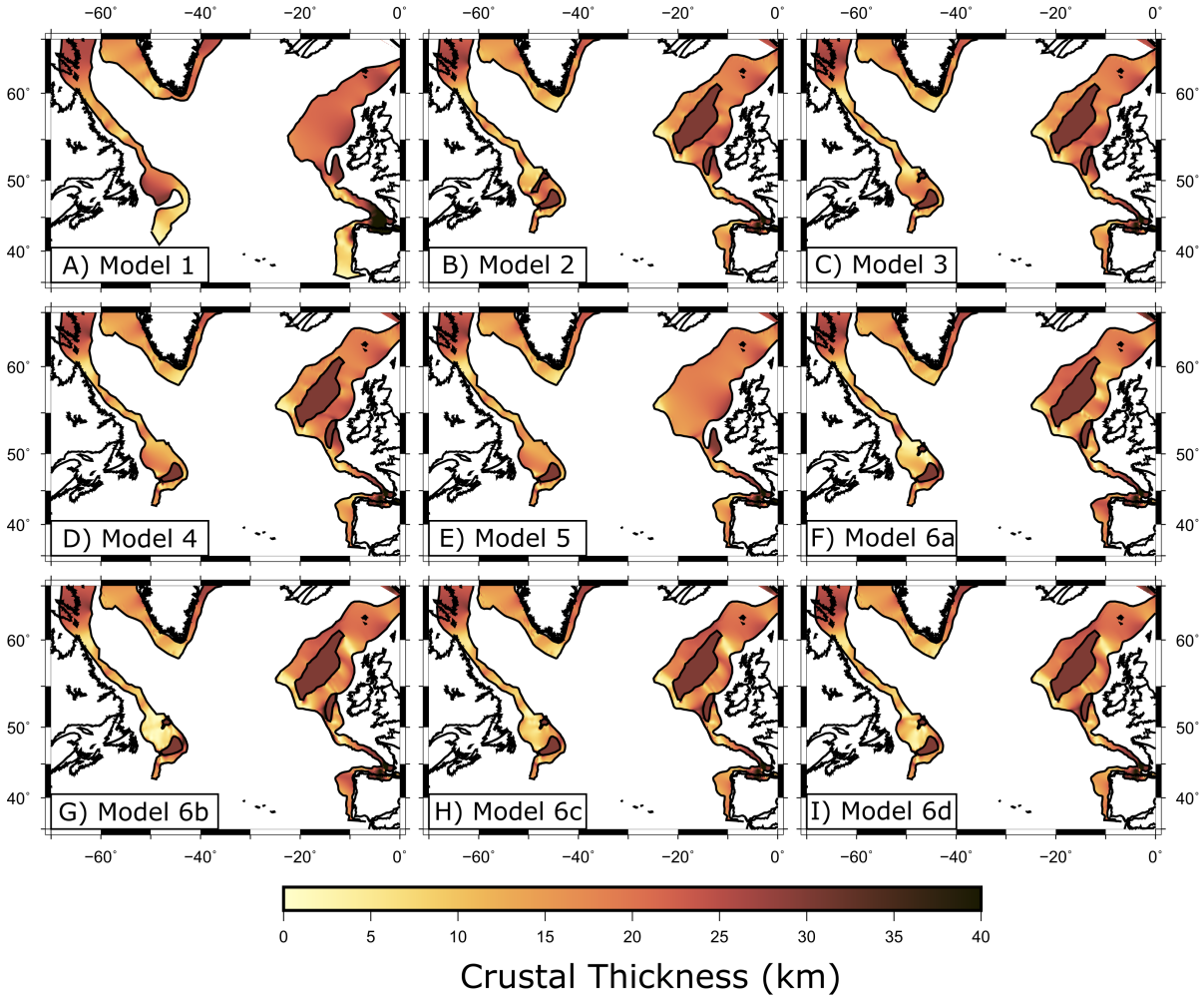

1671

1672 Figure 6 - Modelled crustal thickness at 0 Ma (present) from A) Model 1, B) Model 2, C)
1673 Model 3, D) Model 4, E) Model 5, F) Model 6a, G) Model 6b, H) Model 6c and I) Model 6d.

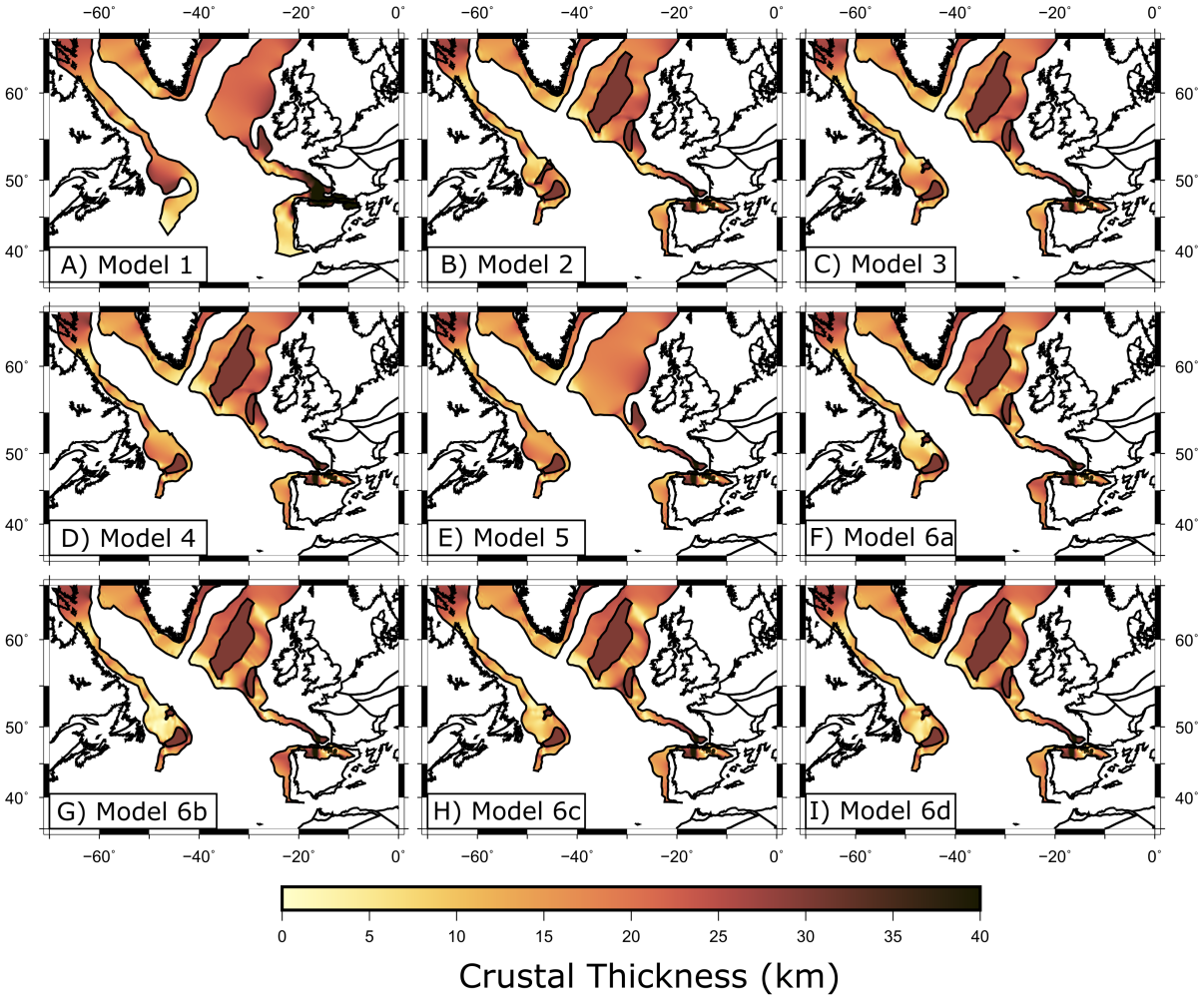

1674

1675 Figure 7 – Modelled crustal thickness at 50 Ma from A) Model 1, B) Model 2, C) Model 3, D)
1676 Model 4, E) Model 5, F) Model 6a, G) Model 6b, H) Model 6c and I) Model 6d.

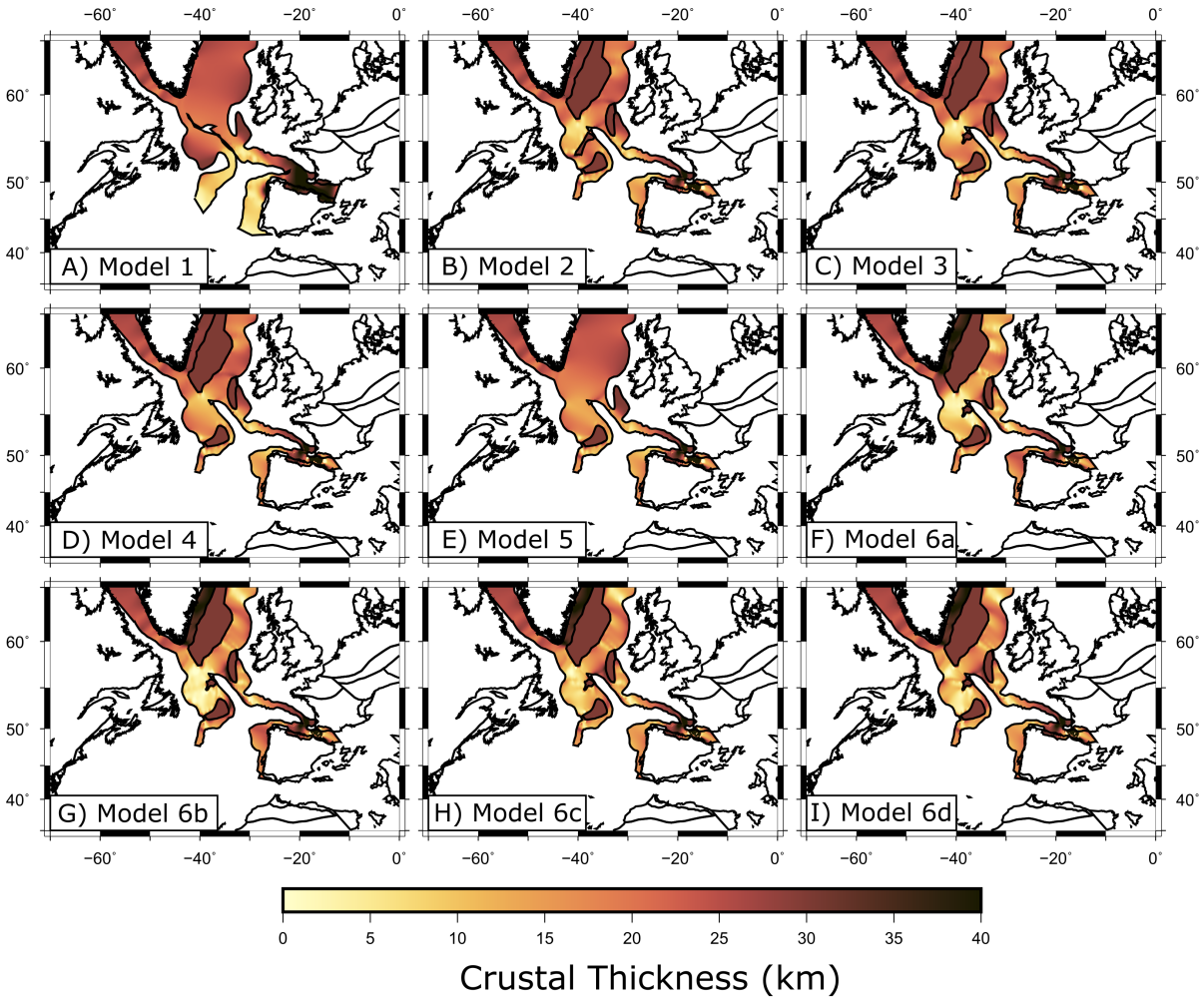

Figure 8 - Modelled crustal thickness at 100 Ma from A) Model 1, B) Model 2, C) Model 3, D) Model 4, E) Model 5, F) Model 6a, G) Model 6b, H) Model 6c and I) Model 6d.

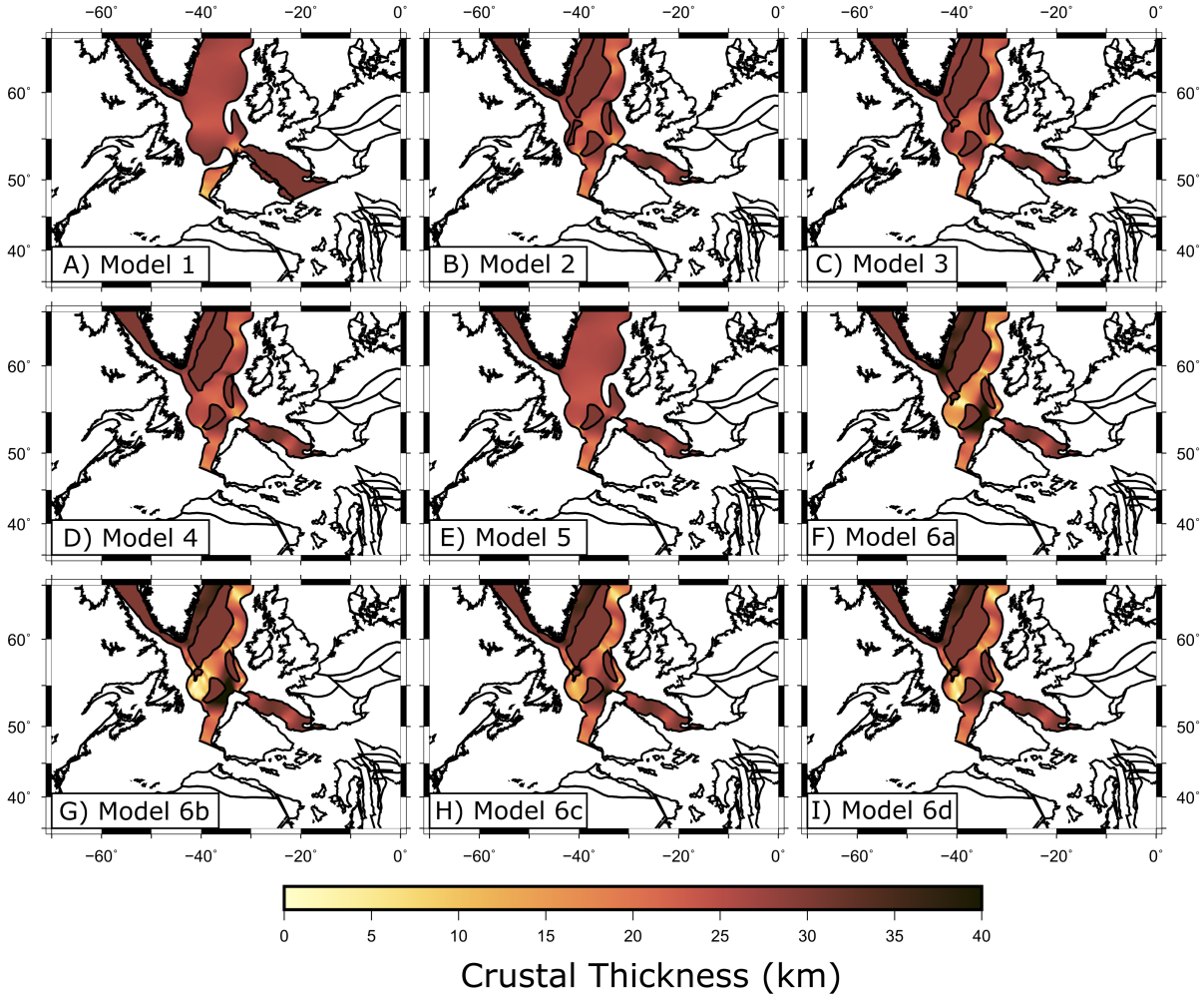

Figure 9 - Modelled crustal thickness at 150 Ma from A) Model 1, B) Model 2, C) Model 3, D) Model 4, E) Model 5, F) Model 6a, G) Model 6b, H) Model 6c and I) Model 6d.

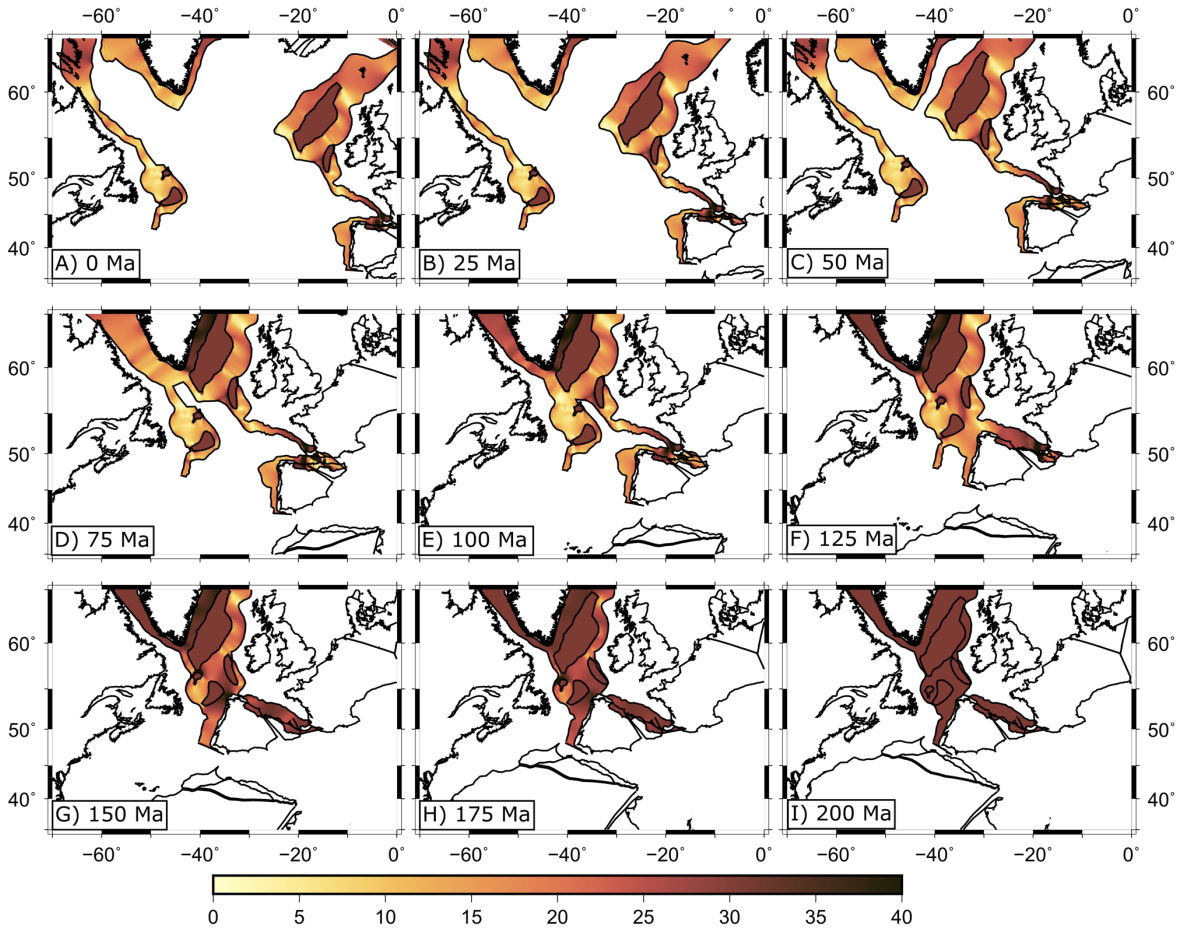

Figure 10 - Temporal evolution of crustal thickness in Model 6c shown at: A) 0 Ma, B) 25 Ma, C) 50 Ma, D) 75 Ma, E) 100 Ma, F) 125 Ma, G) 150 Ma, H) 175 Ma and I) 200 Ma.

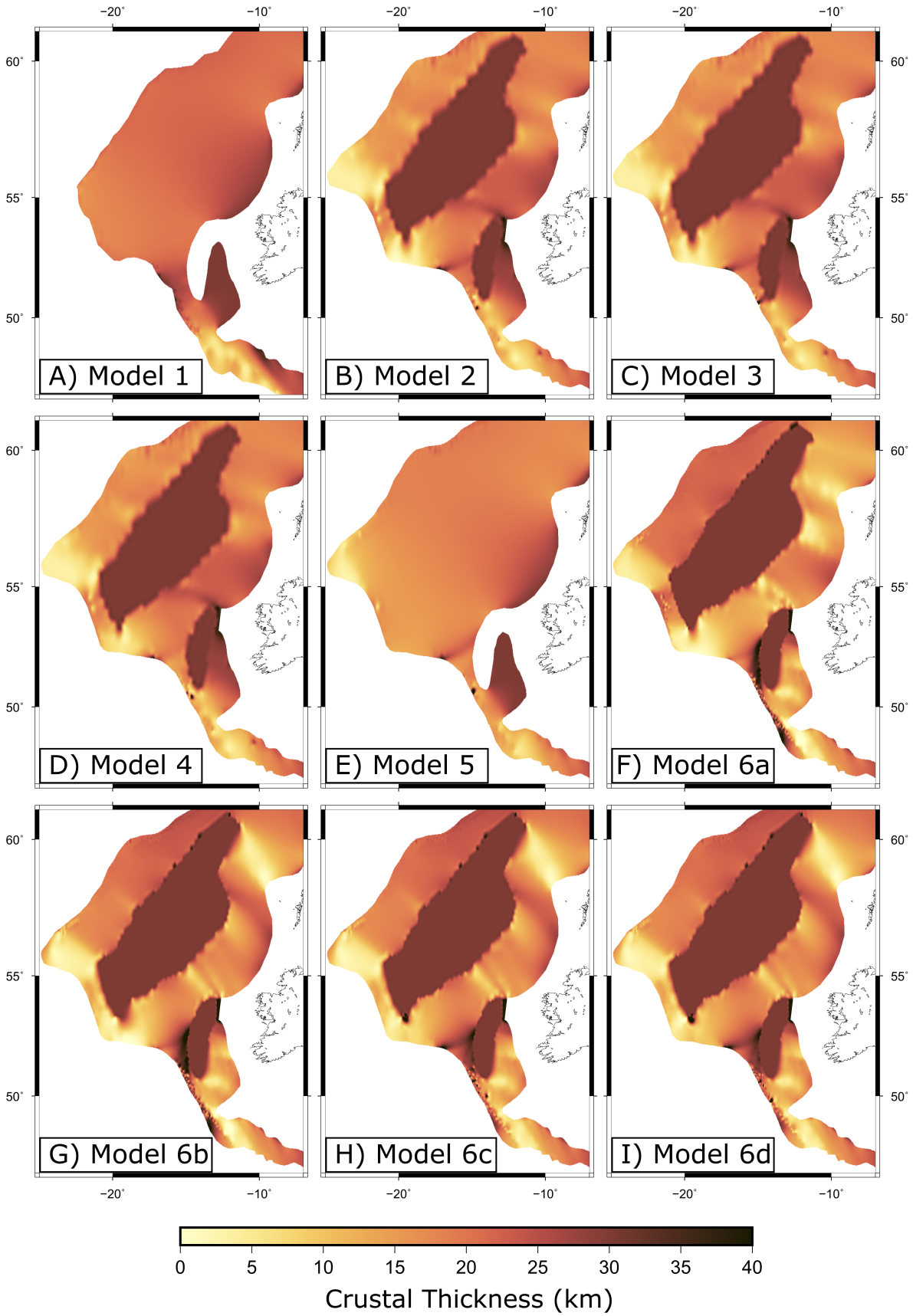

Figure 11 – Irish margin crustal thickness at 0 Ma from A) Model 1, B) Model 2, C) Model 3, D) Model 4, E) Model 5, F) Model 6a, G) Model 6b, H) Model 6c and I) Model 6d.

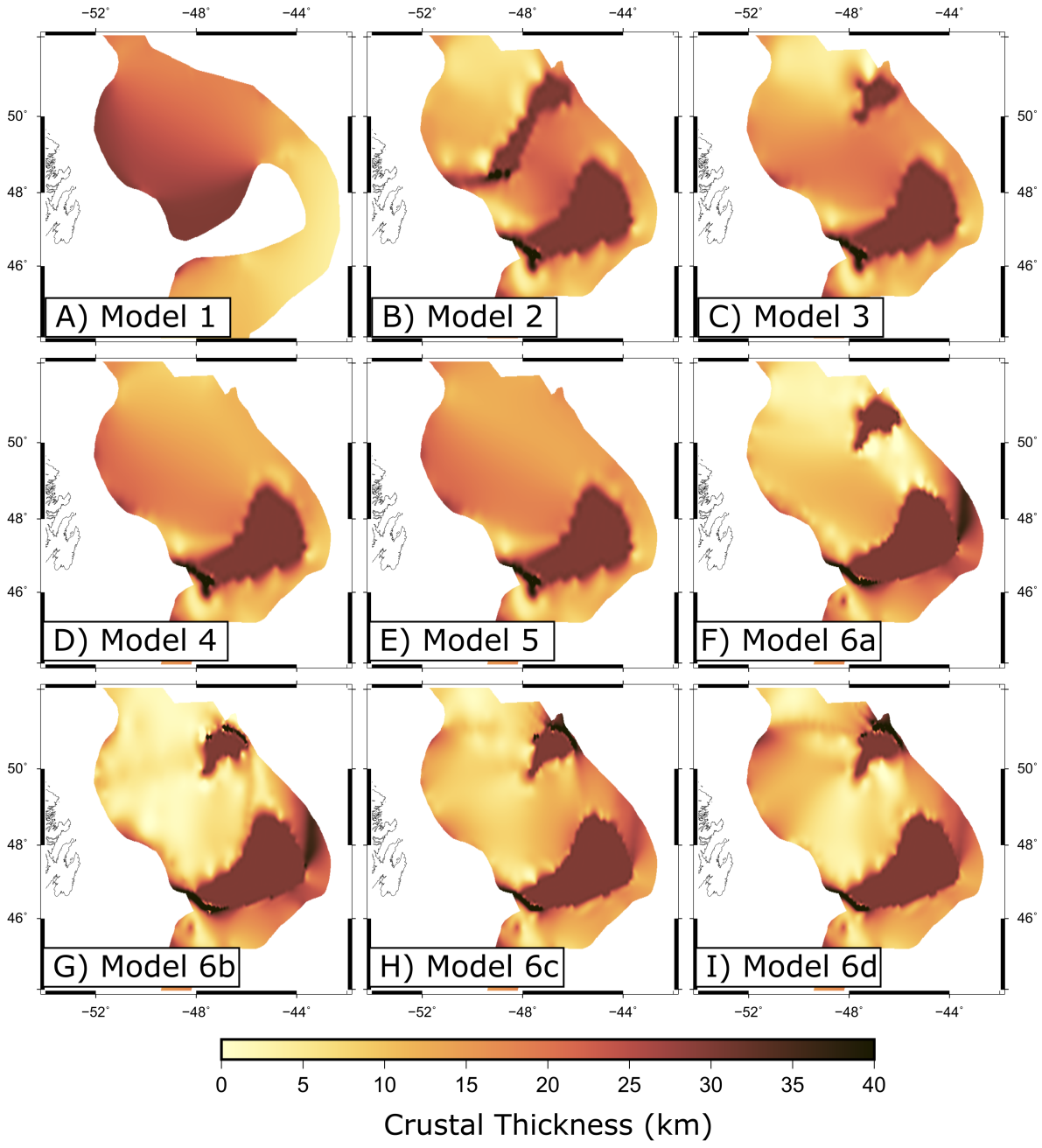

1689

1690 Figure 12 – Newfoundland margin crustal thickness at 0 Ma from A) Model 1, B) Model 2, C)
1691 Model 3, D) Model 4, E) Model 5, F) Model 6a, G) Model 6b, H) Model 6c and I) Model 6d.

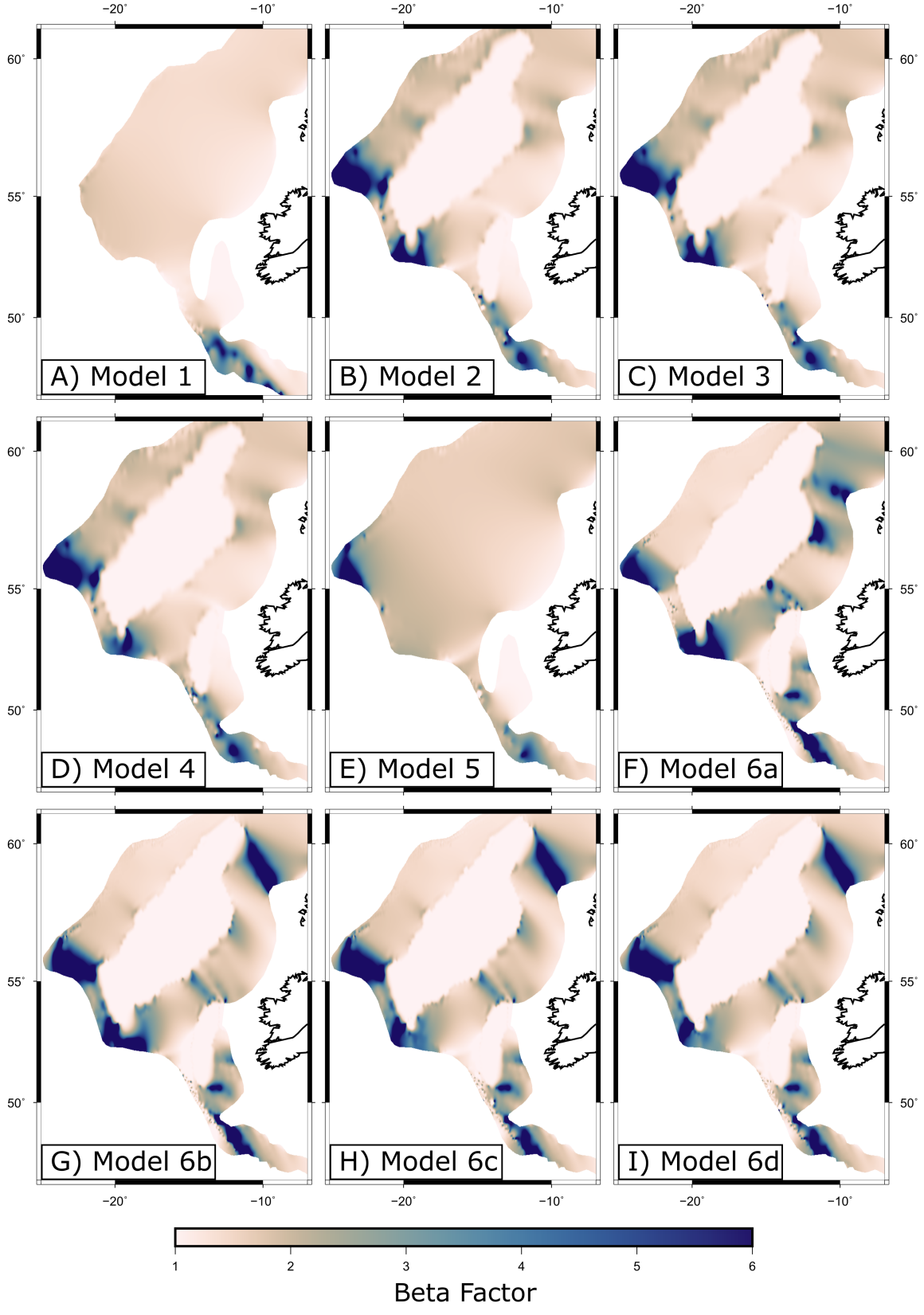

Figure 13 - Irish margin beta factor at 0 Ma from A) Model 1, B) Model 2, C) Model 3, D) Model 4, E) Model 5, F) Model 6a, G) Model 6b, H) Model 6c and I) Model 6d. The beta factor data was cropped at 10 for display.

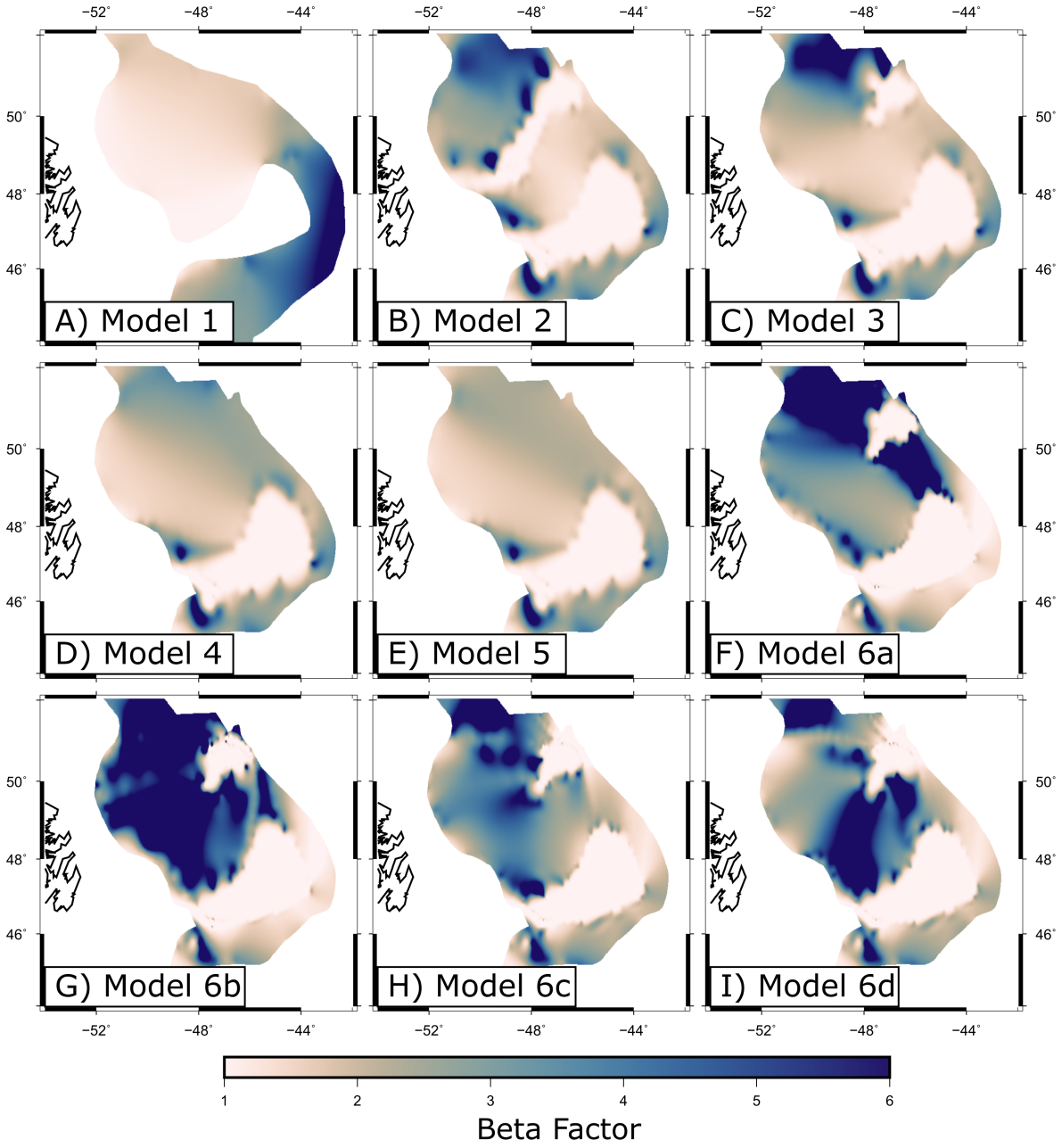

Figure 14 - Newfoundland margin beta factor at 0 Ma from A) Model 1, B) Model 2, C) Model 3, D) Model 4, E) Model 5, F) Model 6a, G) Model 6b, H) Model 6c and I) Model 6d. The beta factor data was cropped at 10 for display.

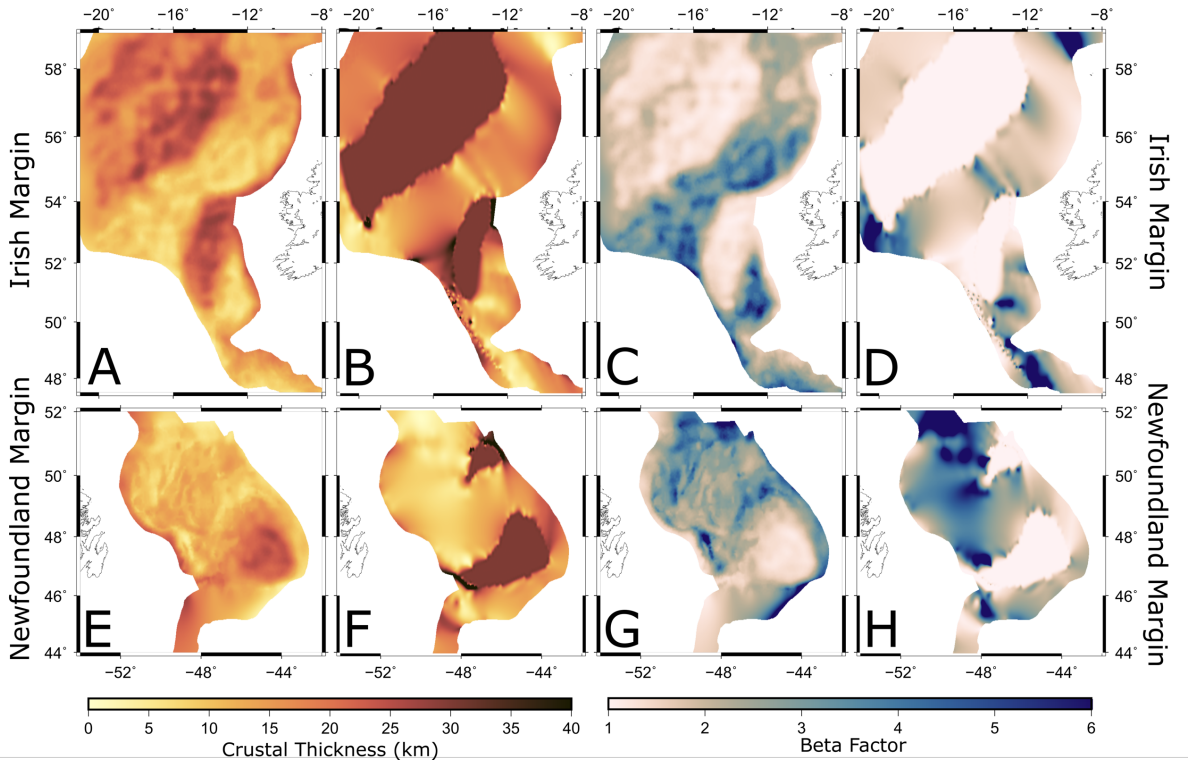

Figure 15 – Irish margin crustal thickness estimate from A) gravity and B) deformable GPlates model 6c and beta factor from C) gravity inversion and D) deformable GPlates models. Newfoundland margin crustal thickness estimate from E) gravity inversion and F) deformable GPlates model 6c and beta factor from G) gravity inversion and H) deformable GPlates model 6c. The gravity inversion for crustal thickness is from Welford et al. (2012). Beta factors were calculated based on a pre-deformation thickness of 30 km. The beta factor data was cropped at 10 for display.

Model #	1	2	3	4	5	6a-d
Inner Boundary	Müller et al. (2016) COBs	Nirrengarten et al. (2018) ECC	Nirrengarten et al. (2018) ECC	Nirrengarten et al. (2018) ECC	Nirrengarten et al. (2018) ECC	Nirrengarten et al. (2018) ECC
Main Outer Boundary	Nirrengarten et al. (2018) Necking Zone (Modified)	Nirrengarten et al. (2018) Necking Zone (Modified)	Nirrengarten et al. (2018) Necking Zone (Modified)	Nirrengarten et al. (2018) Necking Zone (Modified)	Nirrengarten et al. (2018) Necking Zone (Modified)	Nirrengarten et al. (2018) Necking Zone (Modified)
Breakup defined by	Müller et al. (2016) COBs appearance	Nirrengarten et al. (2018) ECC no longer overlapping	Nirrengarten et al. (2018) ECC no longer overlapping	Nirrengarten et al. (2018) ECC no longer overlapping	Nirrengarten et al. (2018) ECC no longer overlapping	Nirrengarten et al. (2018) ECC no longer overlapping
Orphan Knoll	Not included	Separate Plate	Separate Plate with geometry from seismic basement (Fig. 2)	Not included	Not included	Separate Plate with geometry from seismic basement (Fig. 2)
Flemish Cap	Not a separate plate, part of NAM	Separate Plate	Separate Plate	Separate Plate	Separate Plate	Separate Plate
Hatton Bank	Not included	Separate Plate	Separate Plate	Separate Plate	Not included	Separate Plate
Porcupine Bank	Not a separate plate, part of EUR	Separate Plate	Separate Plate	Separate Plate	Not included	Separate Plate with new calculated pole
Davis Strait and Baffin Bay	Welford et al. (2018)	Welford et al. (2018)	Welford et al. (2018)	Welford et al. (2018)	Welford et al. (2018)	Welford et al. (2018)
Poles of rotation	Matthews et al. (2016)	Nirrengarten et al. (2018)	Nirrengarten et al. (2018)	Nirrengarten et al. (2018)	Nirrengarten et al. (2018)	This study (tables 2a-d) after Nirrengarten et al. (2018)
Start time	200 Ma	200 Ma	200 Ma	200 Ma	200 Ma	200 Ma
Original Crustal thickness	30 km	30 km	30 km	30 km	30 km	30 km

Table 1

The components used in Models 1-6(a-d). NAM = North America and EUR = Eurasia.

Age	Latitude	Longitude	Angle	Fixed Plate
Porcupine Bank				
200	53.1758	-11.3586	35.4255	EUR
160	0	0	0	EUR
Rockall-Hatton Bank				
200	51.6692	123.233	-12.4267	GRN
120	50.17	120.8	-12.88	GRN
120	0	0	0	EUR
Flemish Cap				
200	60.1646	-23.7406	77.8799	IB
160	63.94	-20.84	69.15	IB
160	44.65	-54.79	18.83	NAM
140	45.28	-53.47	20.03	NAM
112	0	0	0	NAM
Orphan Knoll				
200	20.8225	-62.6855	4.4293	NAM
140	42.38	-54	12.56	NAM
130	44.97	-52.57	13.2	NAM
112	0	0	0	NAM

Table 2a

Poles of rotation used in Model 6a. All poles not listed are identical to Nirrengarten et al. (2018).

Age	Latitude	Longitude	Angle	Fixed Plate
Porcupine Bank				
200	53.1758	-11.3586	35.4255	EUR
160	0	0	0	EUR
Rockall-Hatton Bank				
200	73.3464	110.659	-16.8172	GRN
120	50.17	120.8	-12.88	GRN
120	0	0	0	EUR
Flemish Cap				
200	61.4116	-23.4066	74.9163	IB
160	63.94	-20.84	69.15	IB
160	44.65	-54.79	18.83	NAM
140	45.28	-53.47	20.03	NAM
112	0	0	0	NAM
Orphan Knoll				
200	44.2801	-46.6569	26.1169	NAM
140	42.38	-54	12.56	NAM
130	44.97	-52.57	13.2	NAM
112	0	0	0	NAM

Table 2b

Poles of rotation used in Model 6b. All poles not listed are identical to Nirrengarten et al. (2018).

Age	Latitude	Longitude	Angle	Fixed Plate
Porcupine Bank				
200	53.1758	-11.3586	35.4255	EUR
160	0	0	0	EUR
Rockall-Hatton Bank				
200	73.3464	110.659	-16.8172	GRN
120	50.17	120.8	-12.88	GRN
120	0	0	0	EUR
Flemish Cap				
200	62.0046	-22.3429	75.2174	IB
160	63.94	-20.84	69.15	IB
160	44.65	-54.79	18.83	NAM
140	45.28	-53.47	20.03	NAM
112	0	0	0	NAM
Orphan Knoll				
200	45.1194	-45.79	26.0864	NAM
140	42.38	-54	12.56	NAM
130	44.97	-52.57	13.2	NAM
112	0	0	0	NAM

Table 2c

Poles of rotation used in Model 6c. All poles not listed are identical to Nirrengarten et al. (2018).

Age	Latitude	Longitude	Angle	Fixed Plate
Porcupine Bank				
200	53.1758	-11.3586	35.4255	EUR
160	0	0	0	EUR
Rockall-Hatton Bank				
200	51.6692	123.233	-12.4267	GRN
120	50.17	120.8	-12.88	GRN
120	0	0	0	EUR
Flemish Cap				
200	62.0046	-22.3429	75.2174	IB
160	63.94	-20.84	69.15	IB
160	44.65	-54.79	18.83	NAM
140	45.28	-53.47	20.03	NAM
112	0	0	0	NAM
Orphan Knoll				
200	46.7381	-45.4488	32.4638	NAM
140	42.38	-54	12.56	NAM
130	44.97	-52.57	13.2	NAM
112	0	0	0	NAM

Table 2d

Poles of rotation used in Model 6d. All poles not listed are identical to Nirrengarten et al. (2018).